Electronic Supplementary Material (ESI) for Dalton Transactions.

Supporting Information

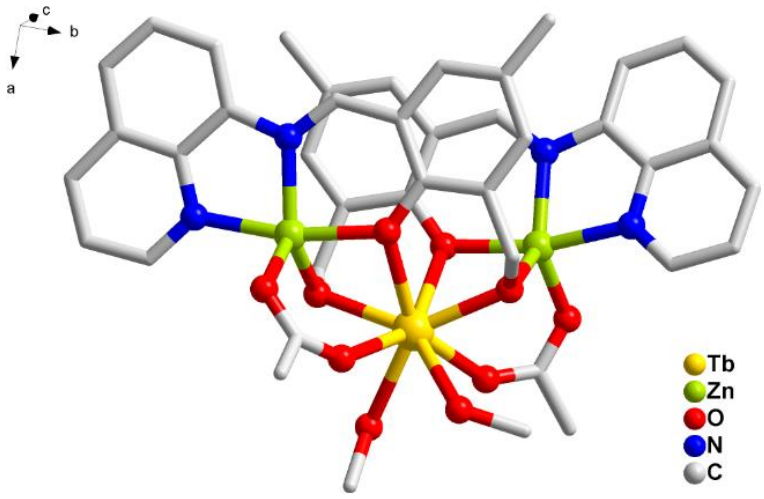

Figure S1. Molecular Structure of **2**. (Nitrate ion and Hydrogen atoms are omitted for clarity)

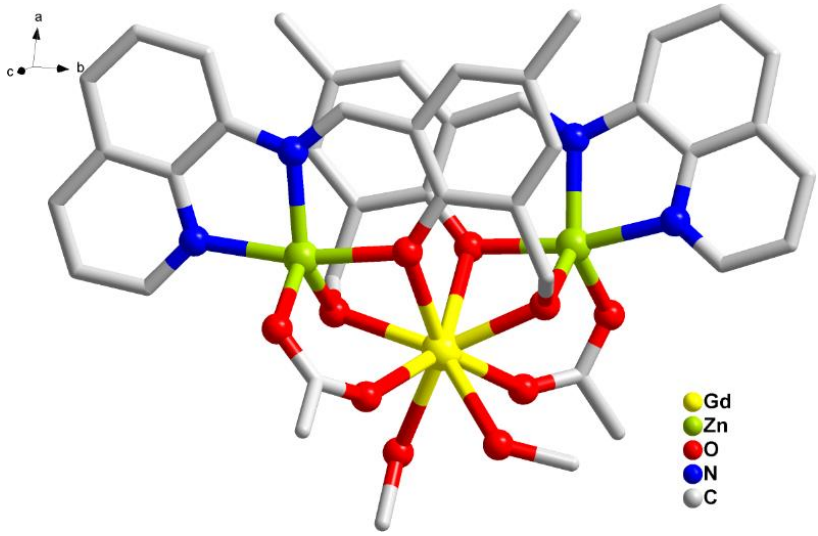

Figure S2. Molecular Structure of **3**. (Nitrate ion and Hydrogen atoms are omitted for clarity)

Table S1. Selected bond distances (Å) and bond angles (°) parameters for **1**.

Bond Lengths around Dysprosium(1)	
Dy(1)-O(3)	2.469(3)
Dy(1)-O(2)	2.272(3)
Dy(1)-O(1)	2.429(4)
Dy(1)-O(4)	2.294(3)
Dy(1)-O(7)	2.340(3)
Dy(1)-O(5)	2.326(3)
Dy(1)-O(9)	2.476(3)
Dy(1)-O(10)	2.449(6)
Bond Lengths around Zinc (1)	
Zn(1)-O(1)	2.111(3)
Zn(1)-O(4)	1.990(3)
Zn(1)-O(6)	2.022(3)
Zn(1)-N(1)	2.133(4)
Zn(1)-N(2)	2.081(4)

Bond Lengths around Zinc (2)	
Zn(2)-O(3)	2.093(3)
Zn(2)-O(2)	1.969(3)
Zn(2)-O(8)	2.012(4)
Zn(2)-N(4)	2.074(4)
Zn(2)-N(3)	2.134(4)
Bond angles	
Zn(1)-O(1)-Dy(1)	93.38(11)
Zn(1)-O(4)-Dy(1)	100.97(13)
Zn(2)-O(3)-Dy(1)	92.30(11)
Zn(2)-Dy(1)-Zn(1)	110.64(3)
Zn(2)-O(2)-Dy(1)	101.93(13)

Table S2. Selected bond distances (Å) and bond angles (°) parameters for **2**.

Bond Lengths around Terbium (1)	
Tb(1)-O(3)	2.296(4)
Tb(1)-O(2)	2.481(4)
Tb(1)-O(1)	2.329(4)
Tb(1)-O(4)	2.431(5)
Tb(1)-O(8)	2.349(4)
Tb(1)-O(5)	2.367(5)
Tb(1)-O(9)	2.462(8)
Tb(1)-O(10)	2.480(4)
Bond Lengths around Zinc (1)	
Zn(1)-O(3)	1.959(4)
Zn(1)-O(2)	2.093(4)
Zn(1)-O(6)	1.999(5)
Zn(1)-N(1)	2.060(5)
Zn(1)-N(2)	2.127(5)

Bond Lengths around Zinc (2)	
Zn(2)-O(4)	2.117(4)
Zn(2)-O(1)	1.979(5)
Zn(2)-O(7)	2.012(4)
Zn(2)-N(4)	2.130(5)
Zn(2)-N(3)	2.057(6)
Bond angles	
Zn(1)-O(1)-Tb(1)	100.83(18)
Zn(1)-O(4)-Tb(1)	93.83(16)
Zn(2)-O(3)-Tb(1)	101.95(18)
Zn(2)-Tb(1)-Zn(1)	110.53(2)
Zn(2)-O(2)-Tb(1)	92.41(15)

Table S3. Selected bond distances (Å) and bond angles (°) parameters for **3**.

Bond Lengths around Gadolinium (1)	
Gd(1)-O(3)	2.331(4)
Gd(1)-O(2)	2.424(4)
Gd(1)-O(1)	2.329(4)
Gd(1)-O(4)	2.274(4)
Gd(1)-O(8)	2.472(3)
Gd(1)-O(5)	2.478(4)
Gd(1)-O(6)	2.340(4)
Gd(1)-O(10)	2.448(6)
Bond Lengths around Zinc (1)	
Zn(1)-O(3)	1.959(4)
Zn(1)-O(9)	1.981(4)
Zn(1)-O(1)	2.012(3)
Zn(1)-N(1)	2.126(4)
Zn(1)-N(2)	2.064(5)

Bond Lengths around Zinc (2)	
Zn(2)-O(8)	2.086(4)
Zn(2)-O(4)	1.964(3)
Zn(2)-O(7)	2.003(4)
Zn(2)-N(4)	2.054(5)
Zn(2)-N(3)	2.128(4)
Bond angles	
Zn(1)-O(9)-Gd(1)	101.30(15)
Zn(1)-O(8)-Gd(1)	92.68(13)
Zn(2)-O(3)-Gd(1)	101.95(18)
Zn(2)-Gd(1) -Zn(1)	110.599(17)
Zn(2)-O(4)-Gd(1)	102.36(15)

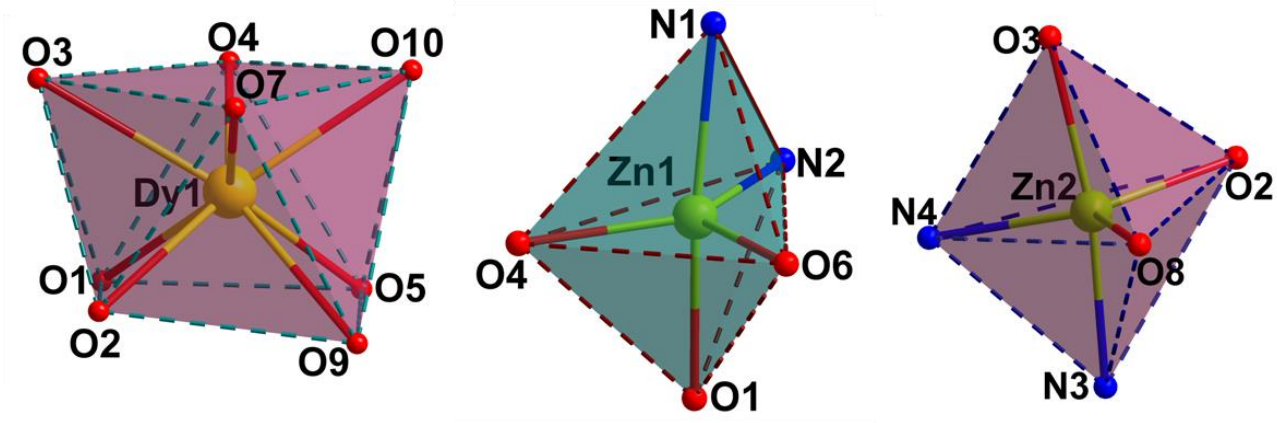

Figure S3. Coordination geometry around Dy^{III} ion and Zn^{II} ions.

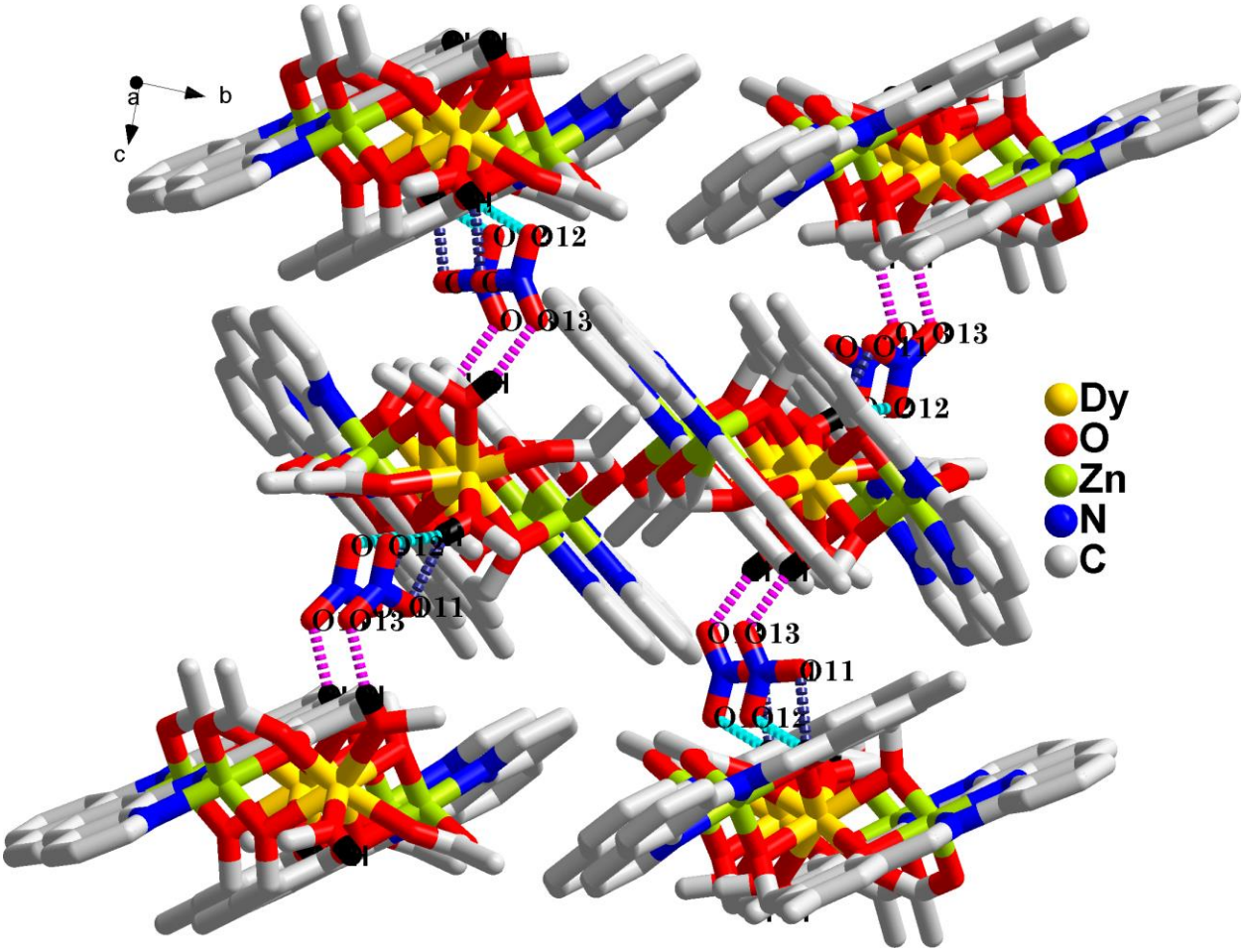

Figure S4. Packing diagram of **1**.

Table S4. Comparison of certain bond length and bond angle of trinuclear Zn-Ln complexes.

Metal complex	Dy-O	Zn-O	Zn-N	Zn-Dy-Zn	Ref
$[DyZn_2(O_2CCMe_3)_6(C_9H_7N)_2(NO_3)]$	2.279(5)-2.464(6)	1.907(5)-1.943(6)	2.082(6)	160.31(2)°	[1]
$[DyZn_2(\mu\text{-}O_2\text{-}CC_2H_5)_5(O_2CC_2H_5)(C_9H_7N)_2(NO_3)(H_2O)]$	2.264(4)-2.520(5)	1.937(4)-1.972(4)	2.060(4)-2.064(4)	137.84(4)°	[1]
$[Zn_2Dy(LH_3)_4]\cdot 3NO_3\cdot 2MeOH\cdot 1.5H_2O$ LH_4 = [2-(2-hydroxy-3-(hydroxymethyl)-5-methylbenzylideneamino)-2-methylpropane-1,3-diol]	2.312(6)-2.408(7)	2.015(8)-2.217(11)	2.049(8)-2.062(9)	177.80°	[2]
$[Zn_2Dy(L_1)_2(OAc)_4](NO_3)_{0.92}(Br)0.08$	2.28(2)-2.55(3)	1.94(1)-2.40(4)	2.01(4)-2.04(4)	175.57(1)	[3]

$[Zn_2Dy(L_1)_2(OAc)_4]ClO_4$	2.28(2)-2.55(1)	1.95(3)-2.40(3)	2.02(3)-2.03(3)	175.59(1)	[3]
$[Zn_2Dy(L_1)_2(OAc)_4]Cl$	2.27(3)-2.51(3)	1.93(4)-2.35(4)	1.98(5)-2.11(10)	171.51(3)	[3]
$[Zn_2Dy(L_1)_2(OAc)_4]PF_6$	2.28(4)-2.50(3)	1.96(4)-2.35(4)	2.00(4)-2.02(4)	168.76(1)	[3]
$[Zn_2Dy(L)(NO_3)_2(OAc)_2(H_2O)]$	2.298(2)-2.502(2)	2.026(3)-2.319(3)	2.014(3)-2.371(3)	46.59°	[4]

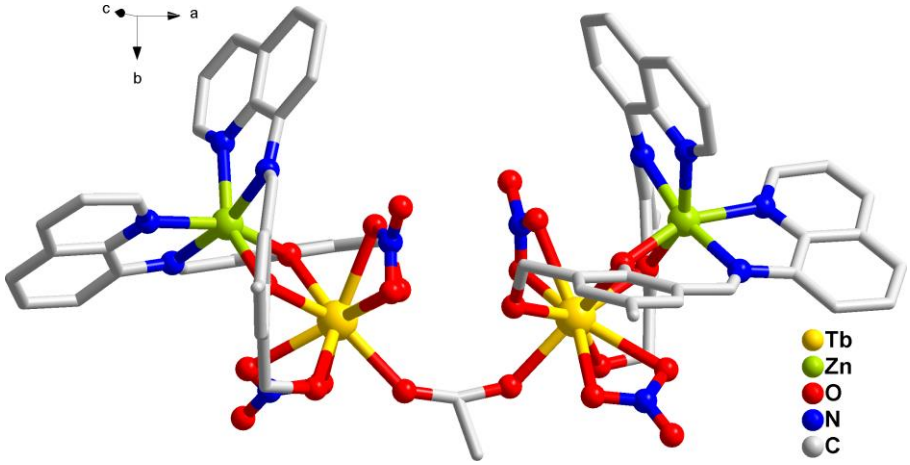

Figure S5. Molecular Structure of **5**. (Nitrate ion and Hydrogen atoms are omitted for clarity)

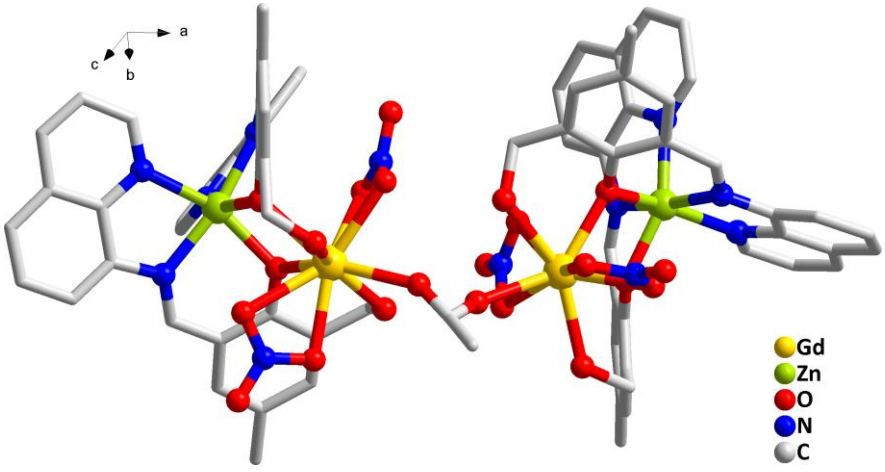

Figure S6. Molecular Structure of **6**. (Nitrate ion and Hydrogen atoms are omitted for clarity)

Table S5. Selected bond distances (Å) and bond angles (°) parameters for **4**.

Bond Lengths around Dysprosium (1)	
Dy(1)-O(3)	2.400(7)
Dy(1)-O(2)	2.298(8)
Dy(1)-O(1)	2.414(6)
Dy (1)-O(4)	2.344(6)
Dy(1)-O(21)	2.311(8)
Dy(1)-O(12)	2.442(6)
Dy(1)-O(13)	2.643(8)
Dy(1)-O(9)	2.428(9)
Dy(1)-O(11)	2.50(1)
Bond Lengths around Dysprosium (2)	
Dy(2)-O(6)	2.368(5)
Dy(2)-O(8)	2.306(4)
Dy(2)-O(22)	2.340(5)
Dy2)-O(7)	2.393(6)
Dy(2)-O(5)	2.409(6)
Dy(2)-O(19)	2.539(6)
Dy(2)-O(15)	2.509(6)
Dy(2)-O(18)	2.426(6)
Dy(2)-O(17)	2.524(6)
Bond Lengths around Zinc (1)	
Zn(1)-O(4)	2.097(8)
Zn(1)-O(2)	2.099(6)
Zn(1)-N(3)	2.128(7)
Zn(1)-N(4)	2.21(1)
Zn(1)-N(2)	2.206(9)
Zn(2)-N(1)	2.122(9)
Bond Lengths around Zinc (2)	
Zn(2)-O(6)	2.134(4)
Zn(2)-O(8)	2.094(5)
Zn(2)-N(5)	2.110(6)
Zn(2)-N(6)	2.239(6)
Zn(2)-N(8)	2.231(8)
Zn(2)-N(7)	2.115(6)
Bond angles	
Zn(1)-O(4)-Dy(1)	106.5(2)
Zn(1)-O(2)-Dy(1)	108.1(2)
Zn(2)-O(6)-Dy(2)	104.84(19)
Zn(2)-O(8)-Dy(1)	108.4(2)

Table S6. Selected bond distances (Å) and bond angles (°) parameters for **5.**

Bond Lengths around Terbium (1)	
Tb(1)-O(8)	2.565(6)
Tb(1)-O(2)	2.314(4)
Tb(1)-O(1)	2.402(4)
Tb (1)-O(4)	2.309(4)
Tb(1)-O(3)	2.450(4)
Bond Lengths around Zinc* (2)	
Zn(1)-O(2)	2.096(4)
Zn(1)-O(4)	2.105(3)
Zn(1)-N(1)	2.129(5)
Zn(1)-N(2)	2.196(5)
Zn(1)-N(3)	2.126(6)
Zn(2)-N(4)	2.182(5)

Tb(1)-O(5)	2.467(6)	**Bond angles**	
Tb(1)-O(6)	2.530(5)	Zn(1)-O(2)-Tb(1)	106.51(2)
Tb(1)-O(11A)	2.351(9)	Zn(1)-O(4)-Tb(1)	106.40(15)
Tb(1)-O(9)	2.428(5)	Zn(1)-O(2)-Tb(2)	106.51(2)
		Zn(1)-O(4)-Tb(2)	106.40(15)
Bond Lengths around Terbium* (2)			
Tb(2)-O(8)	2.565(6)		
Tb(2)-O(2)	2.314(4)		
Tb(2)-O(1)	2.402(4)		
Tb (1)-O(4)	2.309(4)		
Tb(2)-O(3)	2.450(4)		
Tb(2)-O(5)	2.467(6)		
Tb(2)-O(6)	2.530(5)		
Tb(2)-O(11B)	2.36(1)		
Tb(2)-O(9)	2.428(5)		
Bond Lengths around Zinc (1)			
Zn(1)-O(2)	2.096(4)		
Zn(1)-O(4)	2.105(3)		
Zn(1)-N(1)	2.129(5)		
Zn(1)-N(2)	2.196(5)		
Zn(1)-N(3)	2.126(6)		
Zn(2)-N(4)	2.182(5)		

* Symmetry transformations used to generate equivalent atoms: (*) 1-x, y, 0.5-z.

Table S7. Selected bond distances (Å) and bond angles (°) parameters for **6.**

Bond Lengths around Gadolinium (1)		**Bond Lengths around Zinc* (2)**	
		Zn(2)-O(2)	2.096(4)
Gd(1)-O(8)	2.564(7)	Zn(2)-O(4)	2.105(4)
Gd(1)-O(2)	2.314(4)	Zn(2)-N(1)	2.128(5)
Gd(1)-O(1)	2.401(5)	Zn(2)-N(2)	2.196(5)
Gd(1)-O(4)	2.310(4)	Zn(2)-N(3)	2.124(6)
Gd(1)-O(3)	2.450(4)	Zn(2)-N(4)	2.180(5)
Gd(1)-O(5)	2.468(7)	**Bond angles**	
Gd(1)-O(6)	2.531(5)	Zn(1)-O(2)-Gd(1)	106.50(16)
Gd(1)-O(11A)	2.36(1)	Zn(1)-O(4)-Gd(1)	106.35(15)
Gd(1)-O(9)	2.429(5)	Zn(1)-O(2)-Gd(2)	106.50(16)
		Zn(1)-O(4)-Gd(2)	106.35(15)
Bond Lengths around Gadolinium* (2)			
Gd(2)-O(8)	2.564(7)		
Gd(2)-O(2)	2.314(4)		
Gd(2)-O(1)	2.401(5)		

Gd(1)-O(4)	2.310(4)	
Gd(2)-O(3)	2.450(4)	
Gd(2)-O(5)	2.468(7)	
Gd(2)-O(6)	2.531(5)	
Gd(2)-O(11B)	2.3512	
Gd(2)-O(9)	2.429(5)	
Bond Lengths around Zinc (1)		
Zn(1)-O(2)	2.096(4)	
Zn(1)-O(4)	2.105(4)	
Zn(1)-N(1)	2.128(5)	
Zn(1)-N(2)	2.196(5)	
Zn(1)-N(3)	2.124(6)	
Zn(2)-N(4)	2.180(5)	

* Symmetry transformations used to generate equivalent atoms: (*) 1-x, y, 0.5-z.

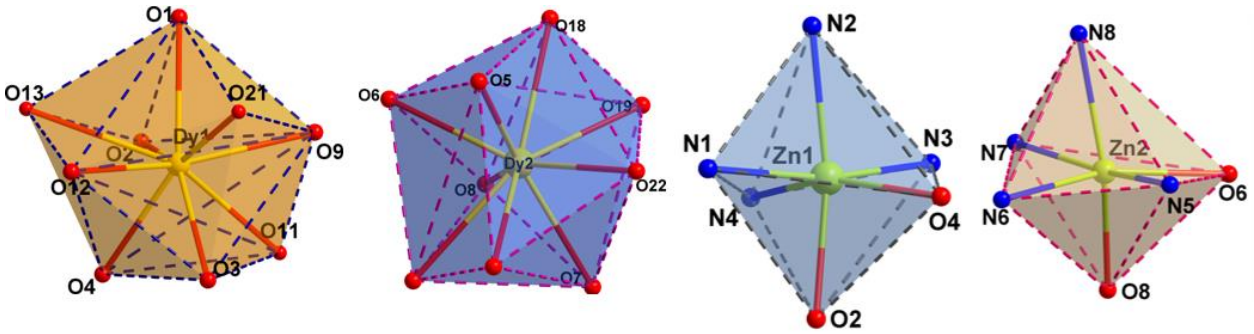

Figure S7. Coordination geometry around metal ions in tetranuclear complex.

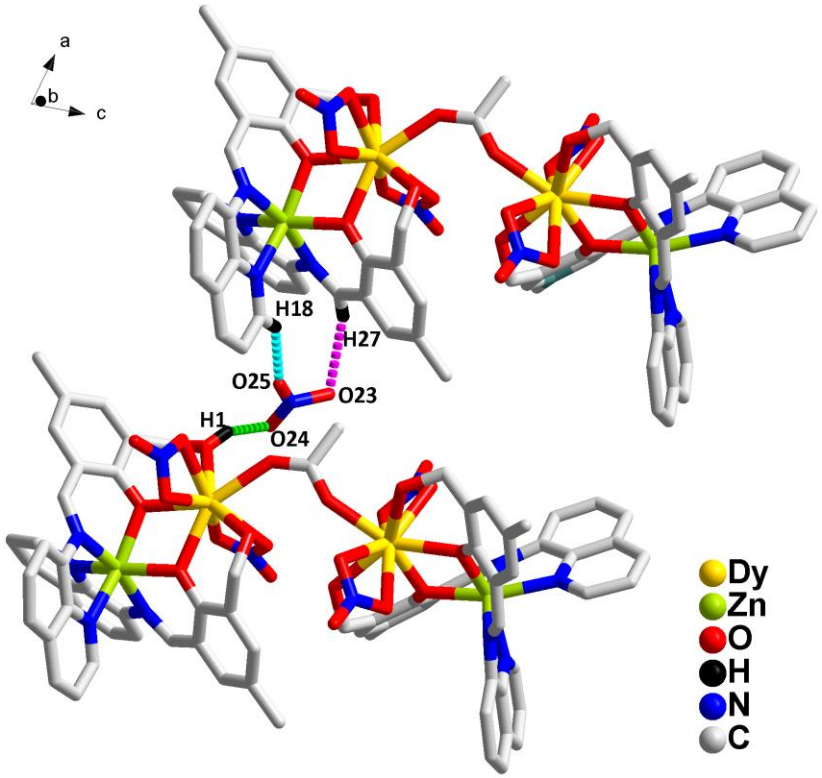

Figure S8. Packing diagram of **4**.

Table S8. Results of the SHAPE measurements for all atoms in Complex **1** and **4**.

Complex **1**													
Sites	OP-8	HPY-8	HBPY-8	CU-8	**SAPR-8**	TDD-8	JGBF-8	JETBPY-8	JBTPR-8	BTPR-8	JSD-8	TT-8	ETBPY-8
Dy1	28.79	22.960	17.542	10.149	**0.423**	2.394	16.033	27.377	2.984	2.344	5.329	10.534	23.072

Sites	PP-5	vOC-5	**TBPY-5**	SPY-5	JTBPY-5
Zn1	28.435	5.140	**1.397**	3.744	3.568
Zn2	28.379	4.882	**1.626**	3.326	3.721

Complex **4**													
Sites	EP-9	OPY-9	HBPY-9	JTC-9	JCCU-9	CCU-9	JCSAPR-9	CSAPR-9	JTCTPR-9	TCTPR-9	JTDIC-9	HH-9	MFF-9
Dy1	36.354	22.435	17.263	15.550	11.058	9.103	3.529	3.044	4.907	3.761	13.260	7.046	**2.204**
Dy2	35.443	22.325	16.511	15.253	10.560	9.526	2.772	2.094	4.105	3.064	12.714	8.369	**1.544**

Sites	HP-6	PPY-6	**OC-6**	TPR-6	JPPY-6
Zn1	33.202	18.289	**3.747**	7.540	22.496

*Abbreviation used: OP-8:Octagon, HPY-8:Heptagonal pyramid, HBPY-8:Hexagonal bipyramid, CU-8:Cube, SAPR-8:Square antiprism, TDD-8:Triangular dodecahedron, JGBF-8:Johnson gyrobifastigium J26, JETBPY-8:Johnson elongated triangular bipyramid J14, JBTPR-8:Biaugmented trigonal prism J50, BTPR-8:Biaugmented trigonal prism, JSD-8 : Snub diphenoid J84, TT-8: Triakis tetrahedron, ETBPY-8:Elongated trigonal bipyramid, EP-9:Enneagon, OPY-9:Octagonal pyramid, HBPY-9:Heptagonal bipyramid, JTC-9:Johnson triangular cupola J3, JCCU-9:Capped cube J8, CCU-9:Spherical-relaxed capped cube, JCSAPR-9:Capped square antiprism J10, CSAPR-9:Spherical capped square antiprism, JTCTPR-9:Tricapped trigonal prism J51, TCTPR-9:Spherical tricapped trigonal prism, JTDIC-9:Tridiminished icosahedron J63, HH-9:Hula-hoop, MFF-9:Muffin, PP-5: Pentagon, vOC-5:Vacant octahedron, TBPY-5:Trigonal bipyramid, SPY-5:Spherical square pyramid, JTBPY-5:Johnson trigonal bipyramid J12, HP-6:Hexagon, PPY-6: Pentagonal pyramid, OC-6:Octahedron, TPR-6:Trigonal prism, JPPY-6:Johnson pentagonal pyramid J2

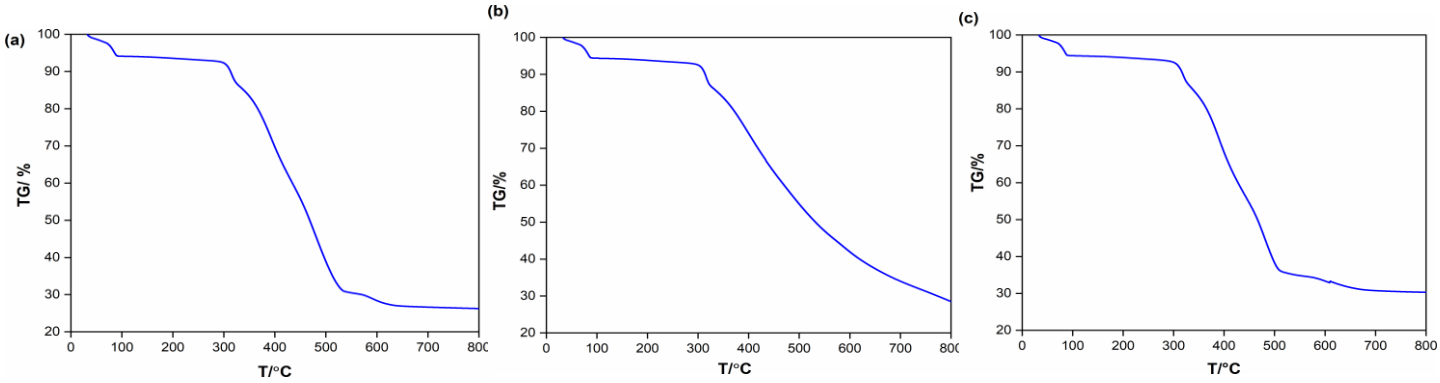

Figure S9. TGA of complex **1-3**.

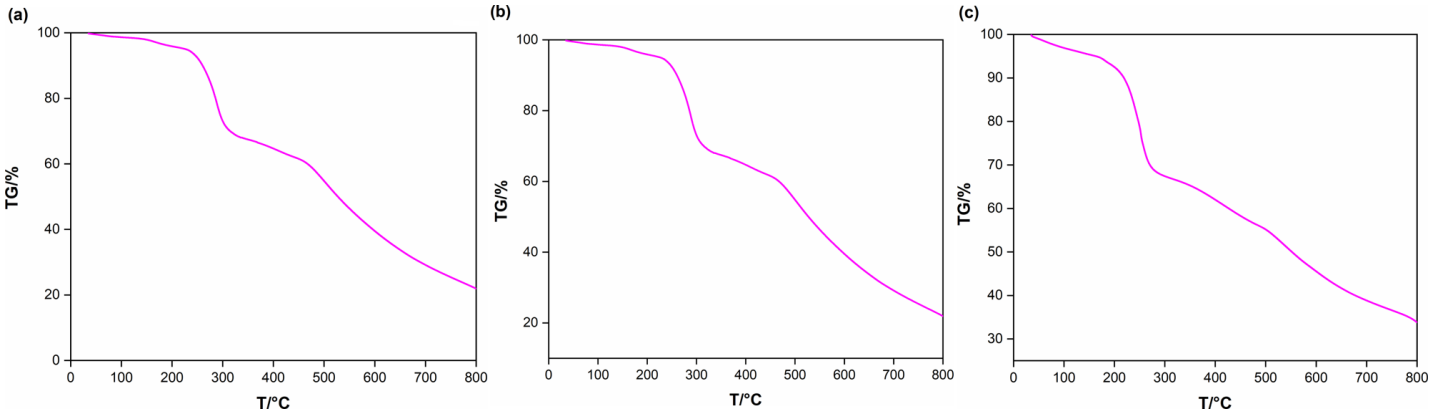

Figure S10. TGA of complex **4-6**.

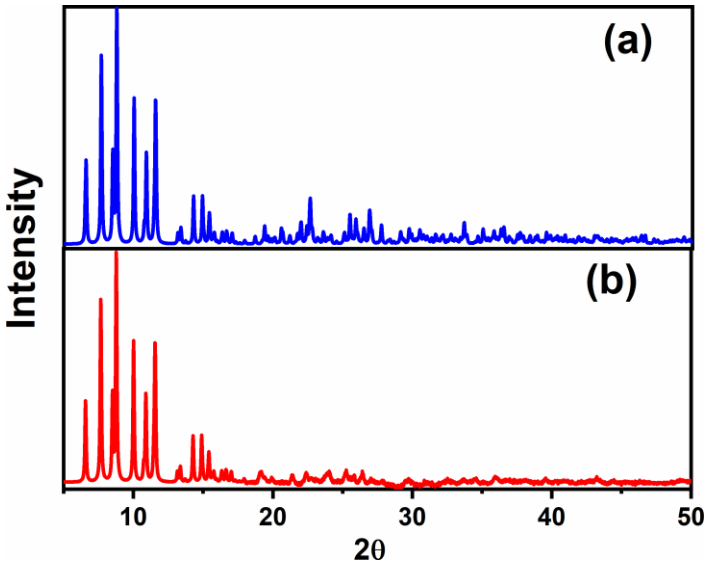

Figure S11. (a) PXRD patterns corresponding to stimulated single crystal data for complex **1**. (b) Experimental PXRD data corresponding to the complex **1**.

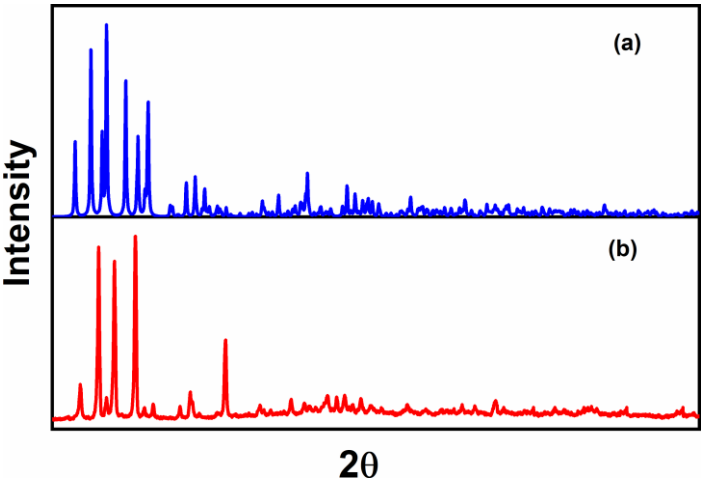

Figure S12. (a) PXRD patterns corresponding to stimulated single crystal data for complex **2**. (b) Experimental PXRD data corresponding to the complex **2**.

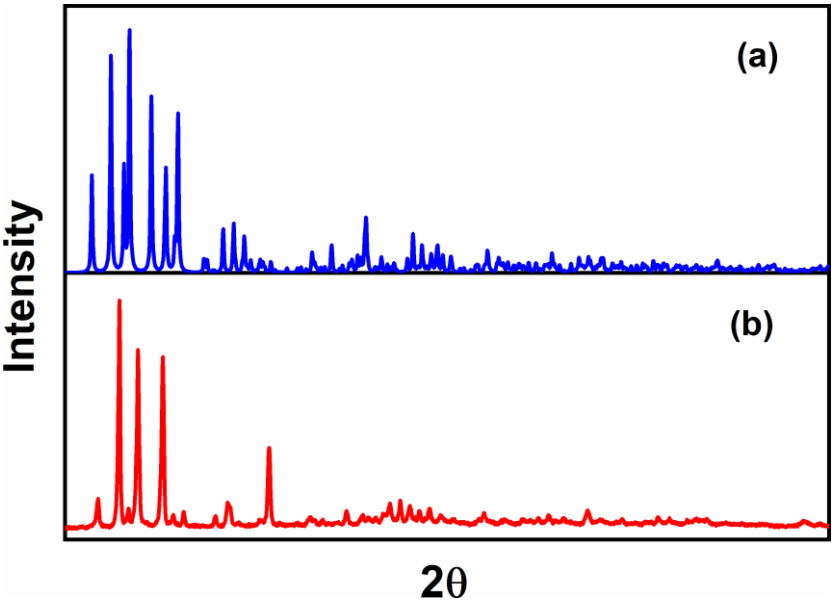

Figure S13. (a) PXRD patterns corresponding to stimulated single crystal data for complex **3**. (b) Experimental PXRD data corresponding to the complex **3**.

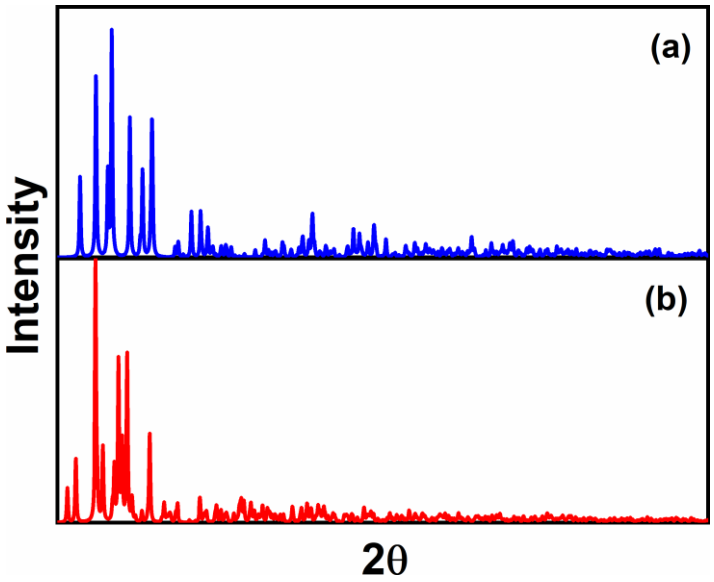

Figure S14. (a) PXRD patterns corresponding to stimulated single crystal data for complex **4**. (b) Experimental PXRD data corresponding to the complex **4**.

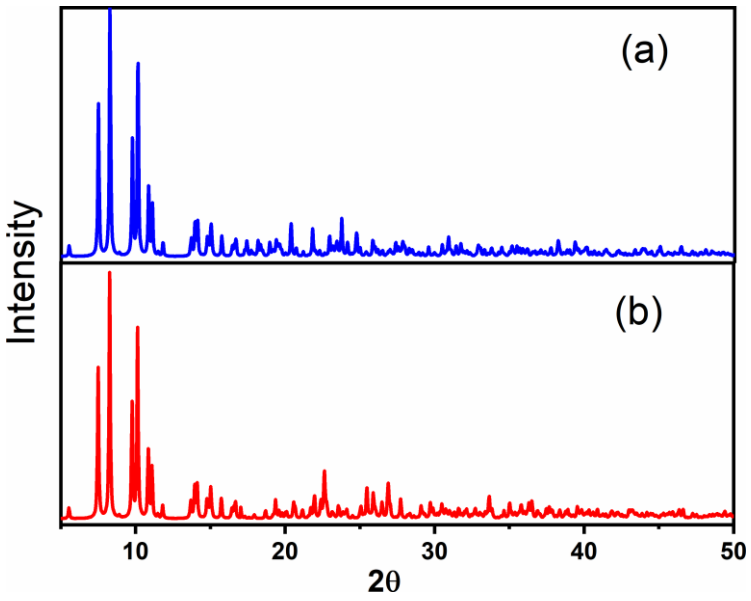

Figure S15. (a) PXRD patterns corresponding to stimulated single crystal data for complex **5**. (b) Experimental PXRD data corresponding to the complex **5**.

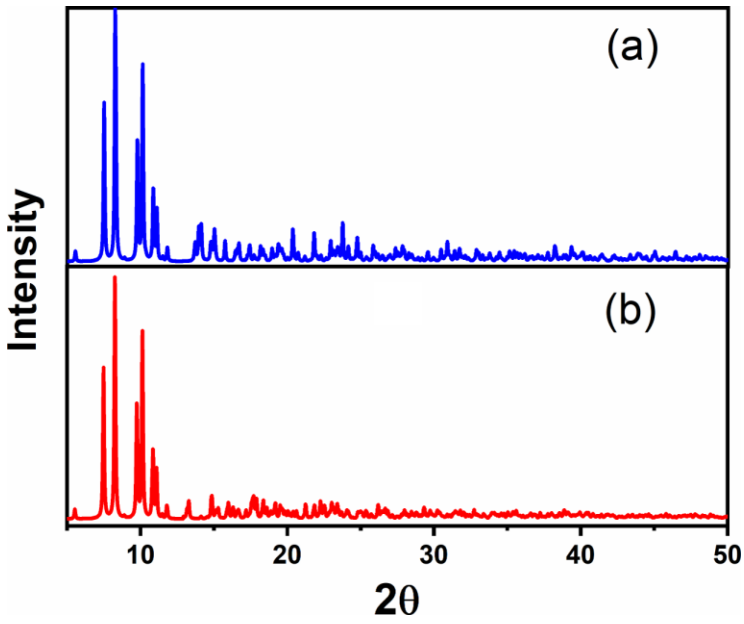

Figure S16. (a) PXRD patterns corresponding to stimulated single crystal data for complex **6**. (b) Experimental PXRD data corresponding to the complex **6**.

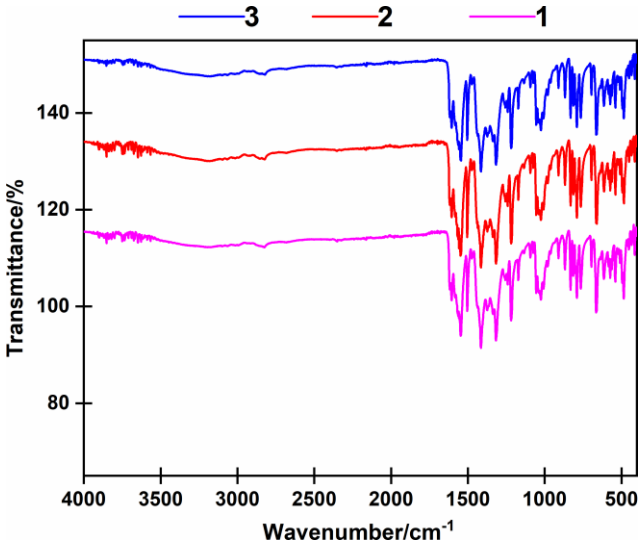

Figure S17. IR of complex **1-3**.

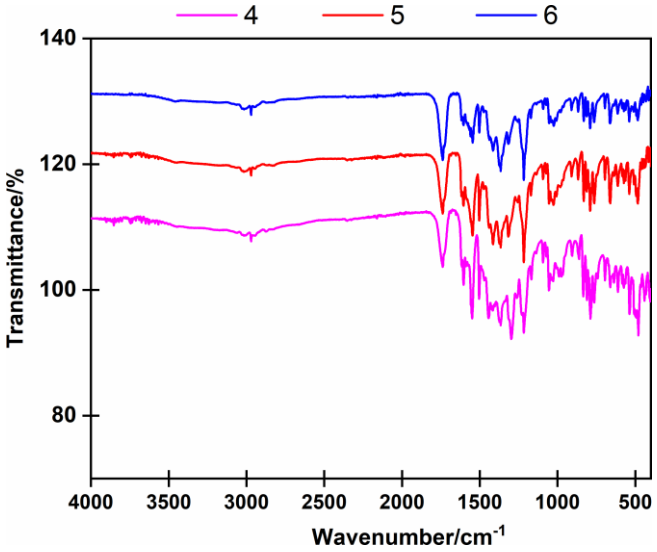

Figure S18. IR of complex **4-6**.

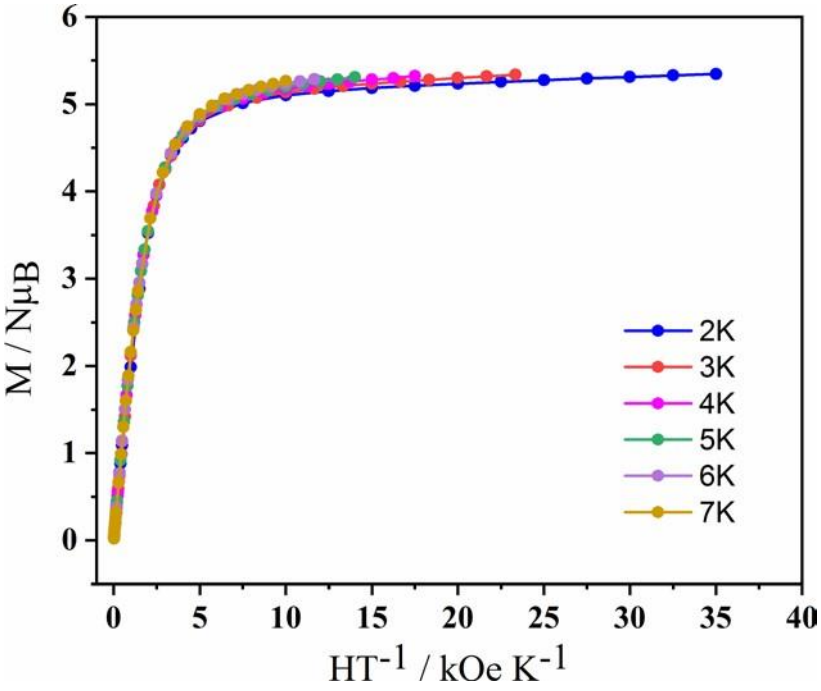

Figure S19. *M* vs. *H*/*T* measurements for compound **1**.

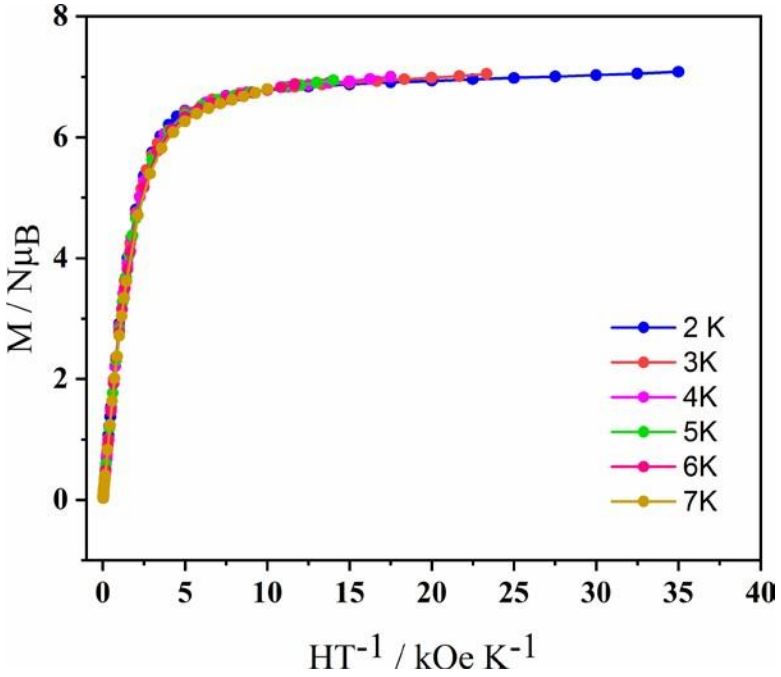

Figure S20. *M* vs. *H*/*T* measurements for compound **2**.

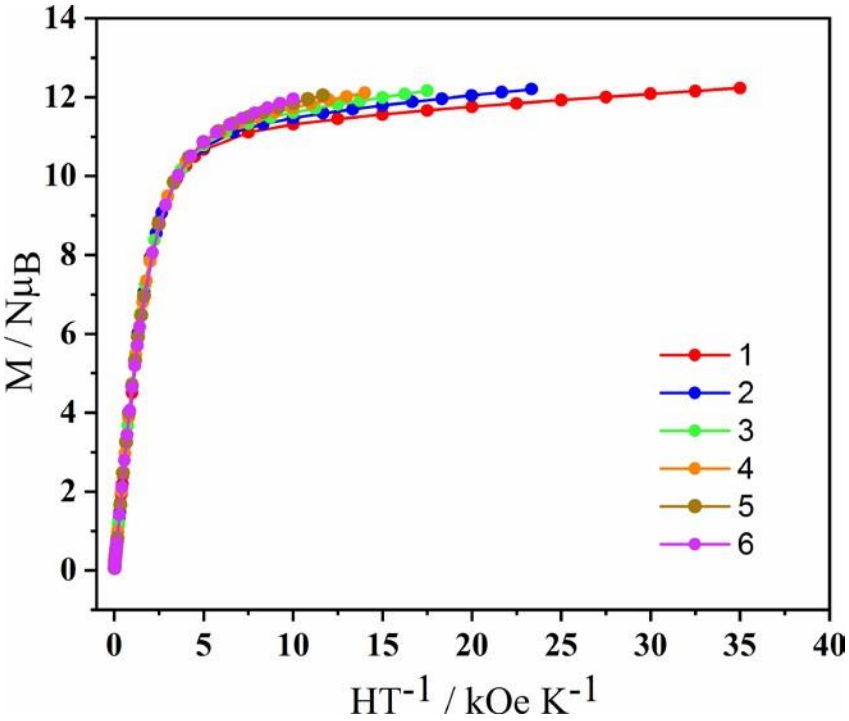

Figure S21. *M* vs. *H*/*T* measurements for compound **4**.

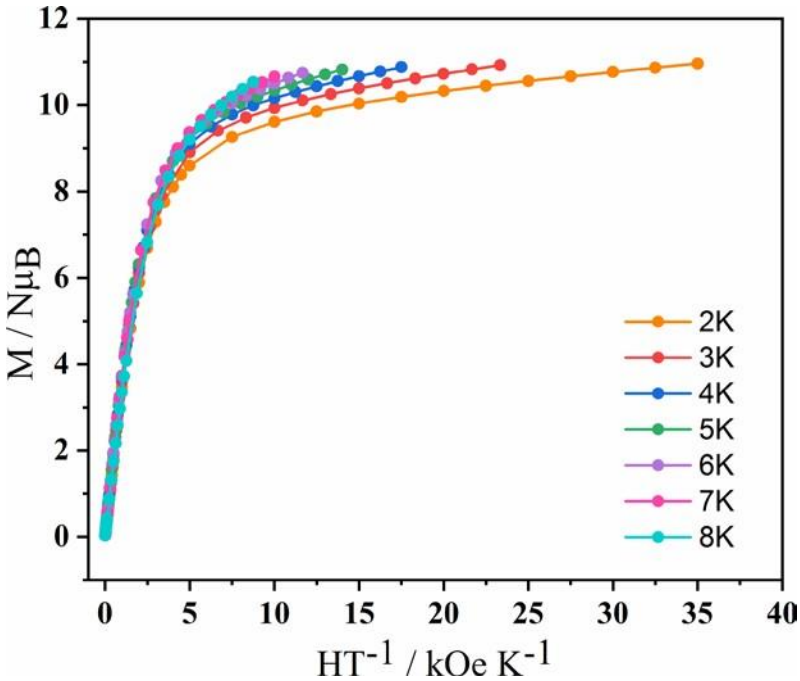

Figure S22. *M* vs. *H*/*T* measurements for compound **5**.

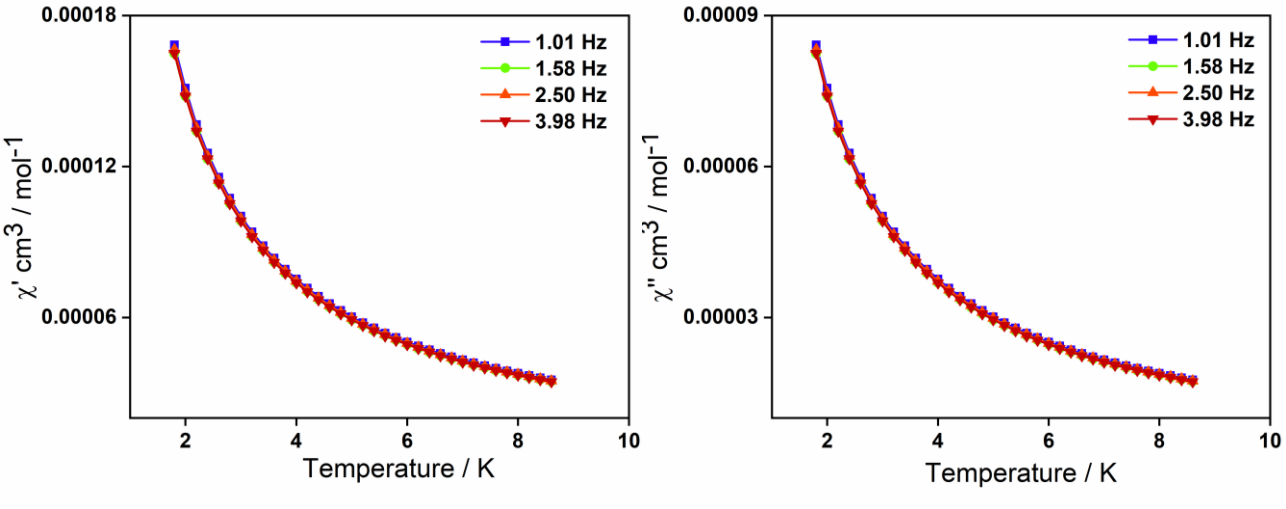

Figure S23. Temperature dependence of out-of-phase ac magnetic susceptibility signals under 0 Oe dc field for **2**.

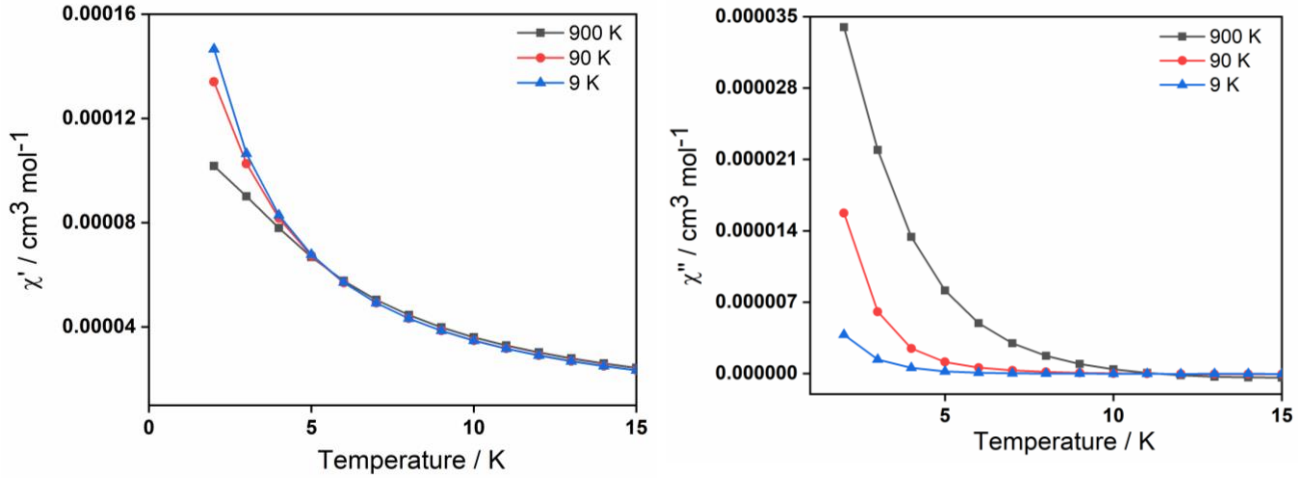

Figure S24. Temperature dependence of out-of-phase ac magnetic susceptibility signals under 1500 Oe dc field for **2**.

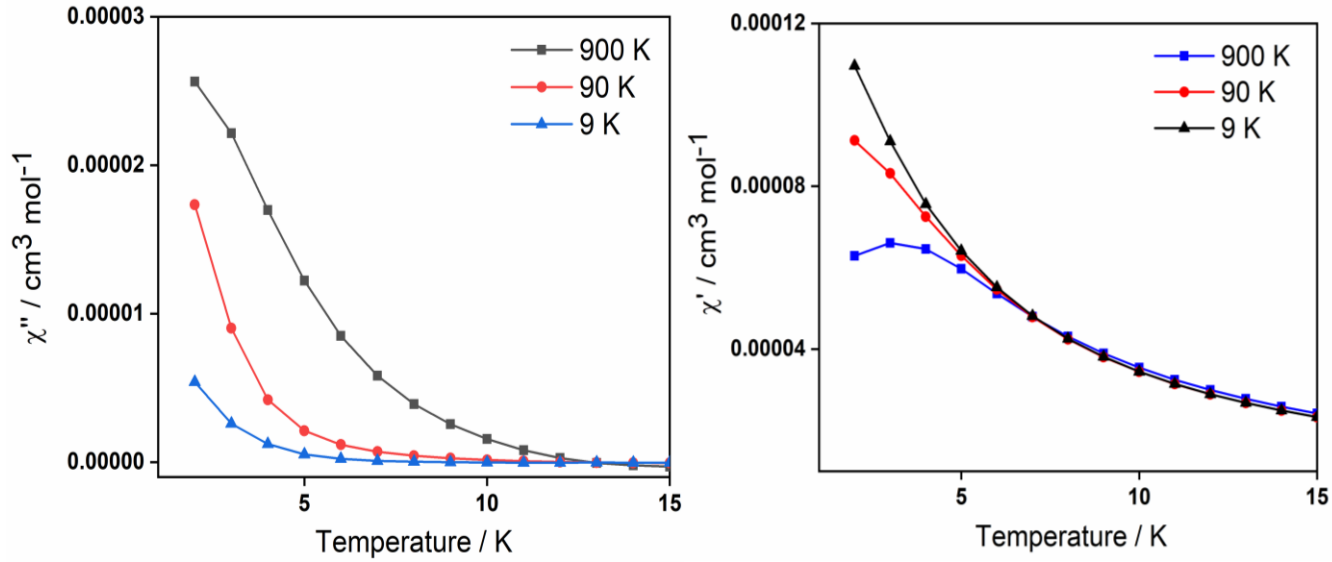

Figure S25. Temperature dependence of out-of-phase ac magnetic susceptibility signals under 2500 Oe dc field for **2**.

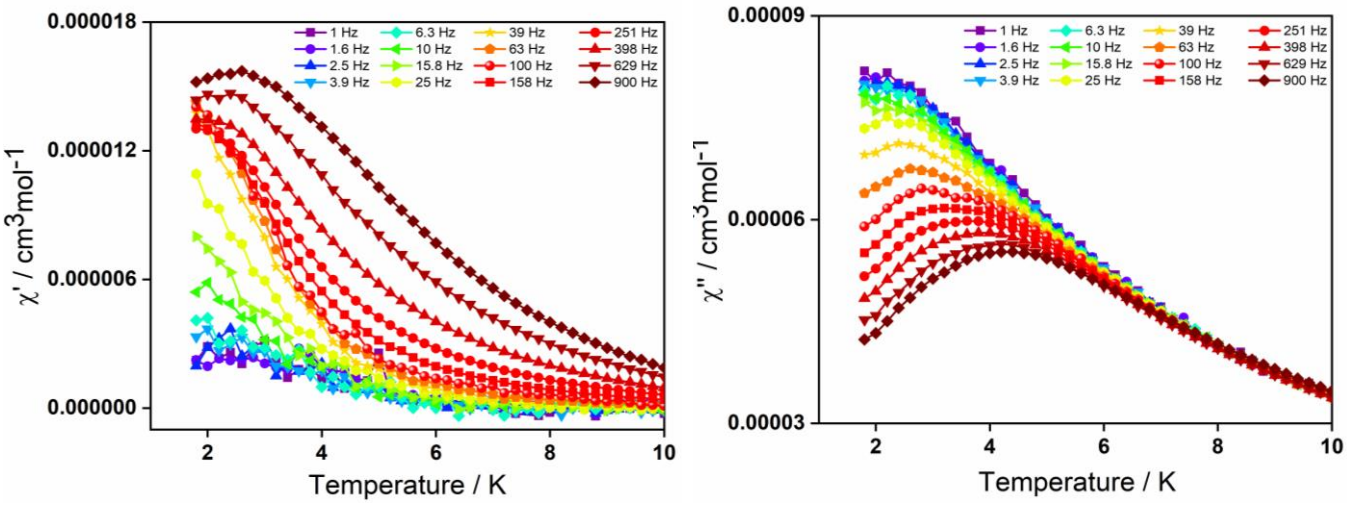

Figure S26. Temperature dependence of out-of-phase ac magnetic susceptibility signals under 3500 Oe dc field for **2**.

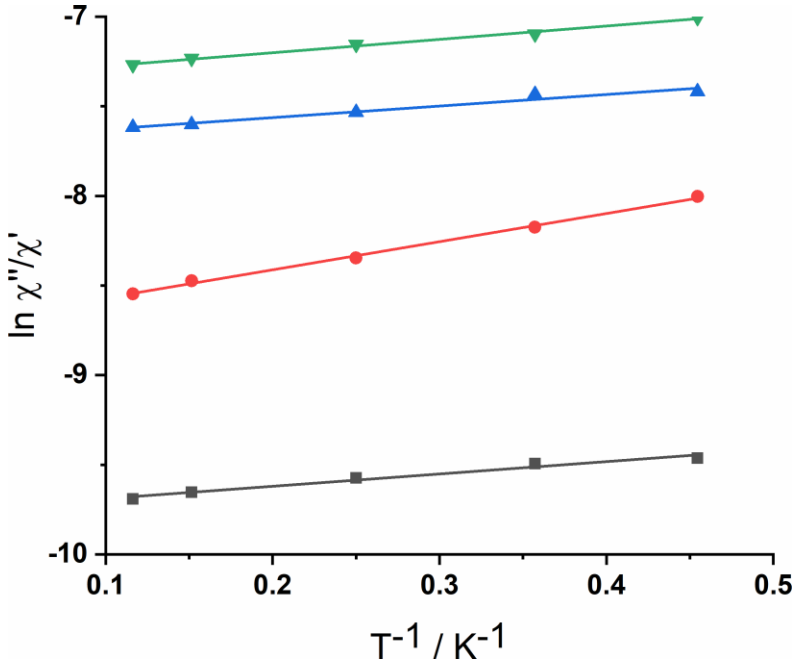

Figure S27. ln(χ′′/χ′) vs. T^{-1} plots at different frequencies; the lines represent the fitting curves for complex **2**.

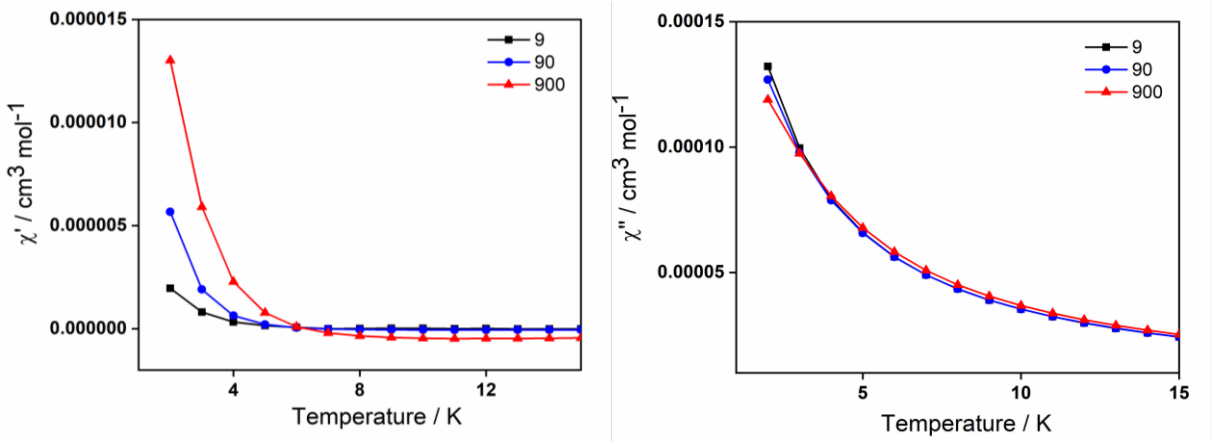

Figure S28. Temperature dependence of out-of-phase ac magnetic susceptibility signals under 2500 Oe dc field for **5**.

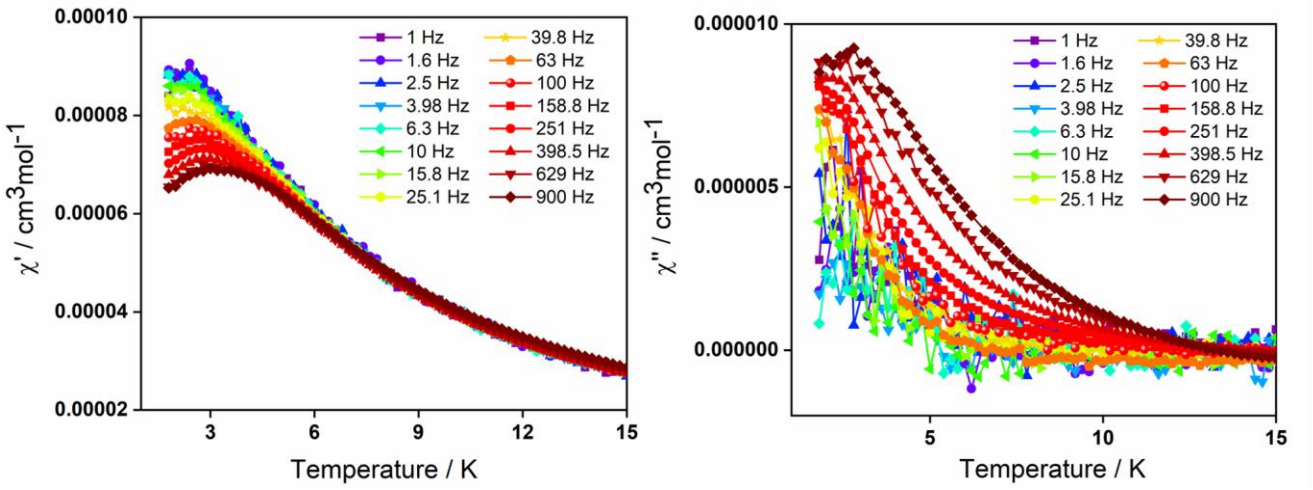

Figure S29. Temperature dependence of out-of-phase ac magnetic susceptibility signals under 3500 Oe dc field for **5**.

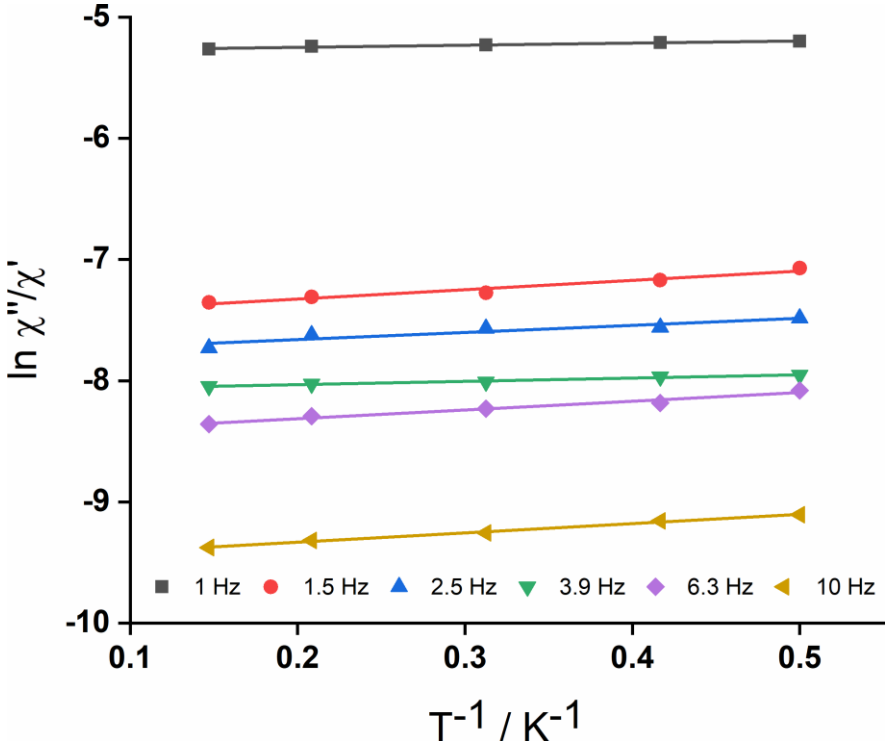

Figure S30. ln(χ″/χ′) vs. T^{-1} plots at different frequencies; the lines represent the fitting curves for complex **5**.

Table S9. List of magnetic properties of selected trinuclear and tetranuclear complexes from the literature

Compounds	Nuclearity	Magnetization behavior	Energy barrier U_{eff}/	Reference
$[Zn_2Dy(L)(NO_3)_3(OH)]$	Trinuclear	Field induced SMM	59 K/ 4.17×10^{-7} s	[5]
$[(LZn(H_2O))_2Dy(H_2O)](CF_3SO_3)_3$ (L^{2-} is the di-deprotonated form of *N*, *N*`-2,2-dimethylpropylenedi(3-methoxysalicylideneiminato)	Trinuclear	SMM	At 0 dc field: 96.9 K /$\tau_0=2.4\times 10^{-7}$ s At 1000 dc field: 128.6K $\tau_0=1.8\times10^{-8}$ s	[6]
$[(LZnBr)_2Dy(H_2O)](ClO_4)$	Trinuclear	SMM	At 0 dc field: 146.8 K/ $\tau_0=9.2\times 10^{-8}$ s	[6]

(L^{2-} is the di-deprotonated form of *N*, *N*`-2,2-dimethylpropylenedi(3-methoxysalicylideneiminato)			At 1000 dc field: 214.7 K /τ_0=9.8× 10^{-9} s	
$[(LZnCl)_2Dy(H_2O)](ClO_4)(MeOH)$ (L^{2-} is the di-deprotonated form of *N*, *N*`-2,2-dimethylpropylenedi(3-methoxysalicylideneiminato)	Trinuclear	SMM	At 0 dc field: 146.1 K/ τ_0 = 9.9× 10^{-8} s At 1000 dc field: 202.4 K/τ_0=1.5× 10^{-8} s	[6]
$[Zn_2Dy(LH_3)_4]$ LH_4 = [2-(2-hydroxy-3-(hydroxymethyl)-5-methylbenzylideneamino)-2-methylpropane-1,3-diol]	Trinuclear	Field induced SMM	67 K / τ_0 = 4.5 × 10^{-8} s	[7]
$[Zn_2Dy(L_1)_2(OAc)_4]$ (X) where X = $(NO_3)_{0.92}(Br)_{0.08}$, ClO_4, Cl and PF_6	Trinuclear	Field induced SMM	For $(NO_3)_{0.92}(Br)_{0.08}$: 25.4 cm^{-1} /5.2×10^{-8} ; For ClO_4 : 12.9 cm^{-1} / 5.8×10^{-9}; For Cl: 14.08 cm^{-1}/ 3.0×10^{-8} ; For PF_6 : 55.5 cm^{-1} / 1.0× 10^{-10}	[8]
$[Zn_2Dy_2(\mu_3\text{-}L')_2(\mu\text{-}sal)_2(NO_3)(CH_3OH)](NO_3)\cdot 5CH_3OH$ H_2L = *N*,*N*′-dimethyl-*N*,*N*′-bis(2-hydroxy-3-formyl-5-bromobenzyl)ethylenediamine; sal = salicylate	Tetranuclear	No SMM behavior	--	[9]
$\{(\mu_3\text{-}CO_3)_2[Zn(\mu\text{-}L)Dy(NO_3)]_2\}\cdot 4CH_3OH$; H_2L = *N*,*N*′,*N*″-trimethyl-*N*,*N*″-bis(2-hydroxy-3-methoxy-5-methylbenzyl)diethylenetriamine	Tetranuclear	Field induced SMM	24 K / τ_0 = 2.3×10^{-6} s	[10]

$[Zn_2Ln_2L_2Cl_2(acetate)_4(MeOH)_2]$ H_2L = 2-methoxy-6-[{2-(2-hydroxyethylamino)ethylimino}-methyl]phenol	Tetranuclear	No SMM behavior	--	[11]
$[ZnL^1Dy(C_2H_5O)(qua)]_2(CF_3SO_3)_2 \cdot 2C_2H_5OH$ (**1**), $[ZnL^1Dy(CH_3O)(bnz)]_2(CF_3SO_3)_2 \cdot 2CH_3OH$ (**2**), $[ZnL^1Dy(CH_3O)(aca)]_2(CF_3SO_3)_2 \cdot 2CH_3OH$ (**3**), $[ZnL^2Dy(CH_3O)(bnz)]_2(CF_3SO_3)_2 \cdot 2CH_3OH$ (**4**), $[ZnL^2Dy(CH_3O)(aca)]_2(CF_3SO_3)_2 \cdot 2CH_3OH$ (**5**) , and $[ZnL^3Dy(CH_3O)(bnz)]_2(CF_3SO_3)_2 \cdot 2CH_3OH$ (**6**) (HL^1 = *N*,*N*‘-bis(2-hydroxy-3-methoxybenzylidene)-1,2-phenylenediamine, HL^2 = *N*,*N*‘-bis(2-hydroxy-3-methoxybenzylidene)-propane-1,2-diamine, HL^3 = *N*,*N*‘-bis(3-methoxysalicylidene)-1,3-propanediamine, qua = 2-quinolinecarboxylic acid, bnz = benzhydroxamic acid and aca = acetohydroxamic acid)	Tetranuclear	SMM	U_{eff}/k_B = 28.34 K, τ_0 = 1.44×10^{-7} s (**1**), U_{eff}/k_B = 27.61 K, τ_0 = 4.68×10^{-5} s (**2**), U_{eff}/k_B = 34.21 K, τ_0 = 9.52×10^{-5} s (**3**), U_{eff}/k_B = 61.23 K, τ_0 = 9.31×10^{-6} s (**4**), U_{eff}/k_B = 34.54 K, τ_0 = 6.83×10^{-5} s (**5**) and U_{eff}/k_B = 36.03 K, and τ_0 = 9.63×10^{-5} s (**6**)	[12]

Materials and Method

Lanthanide salts and Zinc acetate was received from Sigma Aldrich, India. Tetra butyl ammonium hydroxide (TBA-OH) was obtained from SRL Chemicals, India.

Instrumentation

IR data was recorded with a Diamond ATR module using PerkinElmer Spectrum Two FTIR Spectrometer in the range 450-4500 cm^{-1}. Elemental analysis was performed using Thermoquest CE instrument CHNS-O, EA/110 model.

NMR spectra were recorded by a JEOL JNM LAMBDA 400 model spectrometer operating at 400 MHz.

X-Ray Crystallography

X-Ray diffraction was performed on a Rigaku diffractometer with Mo-Kα radiation at low temperature (λ = 0.71073 Å). SMART[13] program was used for collecting frames of data and for determining the lattice parameters. SAINT[13] program was utilized for obtaining the integration of the intensity of reflections and scaling. SADABS[14] was used for absorption correction while SHELXTL[14,15,16] was used for space group and structure determination. The figures of complexes were generated using Diamond 3.1e software[16]. The structures were solved using direct methods by the program SHELXS-2014[17] and Olex-2 software[18]. Presence of disordered solvent molecules were removed by using "PLATON/ "SQUEEZE"[18,19] program. Total electron per unit cell for **1**-**3** are 68.2, 396.8, 169.6 respectively. For Z = 4, the electron count per molecule corresponds to 17.05 for **1** (1 MeOH), 99.2 for **2** (5 MeOH and 1 H_2O) and 42.4 for **3** (1 MeOH and 1 $CHCl_3$). Similarly, total electron per unit cell for **4**-**6** are 58.1, 312 and 312 respectively. For Z = 2, the electron count per molecule corresponds to 29.05 for **4** (1 MeOH and

1 H_2O), 38 for **5** (1 MeOH and 2 H_2O) and for **6** (1 MeOH and 2 H_2O). Crystal data and cell parameters are depicted in Table 2. The data can be obtained free of cost from Cambridge Crystallographic Data Centre with the deposition number 2194864-2194869 for **1-6** respectively.

Table S10. Details of the data collection and refinement parameters for compounds **1-6**.

	1	**2**	**3**	**4**	**5**	**6**
Empirical formula	$C_{42}H_{42}DyN_5O_{13}Zn_2$	$C_{42}H_{42}N_5O_{13}TbZn_2$	$C_{42}H_{42}GdN_5O_{13}Zn_2$	$C_{74}H_{63}Dy_2N_{13}O_{25}Zn_2$	$C_{74}H_{63}N_{13}O_{25}Tb_2Zn_2$	$C_{74}H_{63}Gd_2N_{13}O_{25}Zn_2$
Formula weight	1118.04	1114.46	1112.79	1990.11	1982.95	1979.61
Temperature/K	100.01	273.15	273.15	297.65	100(2)	100(2)
Crystal system	monoclinic	monoclinic	monoclinic	triclinic	monoclinic	monoclinic
Space group	$P2_1/c$	$P2_1/c$	$P2_1/c$	P-1	C2/c	C2/c
a/Å	12.027(4)	11.9571(9)	11.9328(10)	11.9906(9)	36.348(2)	36.348(2)
b/Å	20.800(6)	20.8492(16)	20.8385(18)	15.9962(11)	12.6844(7)	12.6844(7)
c/Å	18.417(5)	18.1968(15)	18.2495(15)	22.9493(15)	19.8980(11)	19.8980(11)
α/°	90	90	90	76.896(3)	90	90
β/°	106.674(8)	106.113(2)	106.152(2)	75.140(3)	118.758(2)	118.758(2)
γ/°	90	90	90	83.179(4)	90	90
Volume/Å^3	4414(2)	4358.2(6)	4358.8(6)	4135.2(5)	8042.4(8)	8042.4(8)
Z	4	4	4	2	4	4
ρ_{calc}g/cm^3	1.683	1.699	1.696	1.598	1.638	1.635
μ/mm^{-1}	2.823	2.767	2.666	2.441	2.411	2.302
F(000)	2236.0	2232.0	2228.0	1980.0	3952.0	3944.0
Crystal size/mm^3	0.042 × 0.038 × 0.026	0.045 × 0.036 × 0.028	0.044 × 0.036 × 0.026	0.056 × 0.033 × 0.021	0.264 × 0.223 × 0.181	0.245 × 0.213 × 0.164
Radiation	MoKα (λ = 0.71073)	MoKα (λ = 0.71073)	MoKα (λ = 0.71073)	MoKα (λ = 0.71073)	MoKα (λ = 0.71073)	MoKα (λ = 0.71073)
2Θ range for data collection/°	4.12 to 50.998	4.55 to 50.998	4.548 to 56.608	4.056 to 50.992	4.674 to 50.696	4.674 to 50
Index ranges	-14 ≤ h ≤ 14, -23 ≤ k ≤ 25, -22 ≤ l ≤ 22	-14 ≤ h ≤ 14, -25 ≤ k ≤ 25, -22 ≤ l ≤ 22	-15 ≤ h ≤ 15, -27 ≤ k ≤ 27, -24 ≤ l ≤ 24	-14 ≤ h ≤ 14, -19 ≤ k ≤ 19, -27 ≤ l ≤ 27	-43 ≤ h ≤ 43, -15 ≤ k ≤ 15, -23 ≤ l ≤ 23	-43 ≤ h ≤ 43, -15 ≤ k ≤ 15, -23 ≤ l ≤ 23

Reflections collected	33793	52826	69951	110123	50491	48852
Independent reflections	8209 [R_{int} = 0.0476, R_{sigma} = 0.0387]	8098 [R_{int} = 0.0628, R_{sigma} = 0.0392]	10811 [R_{int} = 0.0766, R_{sigma} = 0.0490]	15403 [R_{int} = 0.0760, R_{sigma} = 0.0491]	7361 [R_{int} = 0.0525, R_{sigma} = 0.0323]	7065 [R_{int} = 0.0513, R_{sigma} = 0.0313]
Data/restraints / parameters	8209/5/574	8098/8/568	10811/6/568	15403/12/1002	7361/0/538	7065/0/527
Goodness-of-fit on F^2	1.037	1.093	1.066	1.082	1.048	1.037
Final R indexes [I>=2σ]	R_1 = 0.0373, wR_2 = 0.0924	R_1 = 0.0471, wR_2 = 0.1260	R_1 = 0.0458, wR_2 = 0.1227	R_1 = 0.0553, wR_2 = 0.1369	R_1 = 0.0406, wR_2 = 0.1089	R_1 = 0.0415, wR_2 = 0.1108
Final R indexes [all data]	R_1 = 0.0429, wR_2 = 0.0963	R_1 = 0.0580, wR_2 = 0.1381	R_1 = 0.0677, wR_2 = 0.1457	R_1 = 0.0889, wR_2 = 0.1707	R_1 = 0.0550, wR_2 = 0.1199	R_1 = 0.0548, wR_2 = 0.1232
Largest diff. peak/hole / e $Å^{-3}$	3.05/-1.93	2.49/-2.2	2.71/-2.14	2.30/-1.30	1.64/-0.90	2.29/-0.59

Magnetic Measurement

The magnetization of powdered sample was measured over the 1.8−300 K temperature range using a Quantum Design SQUID-based MPMSXL-5-type magnetometer. Direct current (dc) measurements were recorded under 1000 Oe magnetic field in the range 300 to 2 K. Field dependent magnetization was recorded in the range of 0 to 7 T at 2 K.

Computational Details

All the calculations have been done on the hydrogens optimized geometry using ORCA/5.0.3.[20] Initially, hydrogen positions were optimized using the BP86 functional and SV basis sets.[21]

Subsequently, these optimized hydrogen coordinates were used for the computation of spin Hamiltonian (SH) parameters.

All Ab initio calculations were carried out using the OpenMOLCAS code.[22] The spin-Hamiltonian parameters for the **1**, **2**, **4**, and **5**, complexes were derived using the complete active space self-consistent field (CASSCF) technique. An active space of CAS (9,7) i.e nine active electrons in the seven active *f*-orbitals of the Dy^{III} ion, was taken into consideration for the complex **1** in order to estimate the spin-Hamiltonian parameters in the Complete Active Space Self-Consistent Field (CASSCF) framework.[23] Similarly, for complex **2**, an active space of CAS (8,7) was used for Tb^{III} ion. Here, we have employed basis set ANO-RCC-VDZP for Ln (III), ANO-RCC-VDZ for C, O, N, and ANO-RCC-MB for H.[24,25] To speed up the calculations, the two-electron integrals were computed using the Resolution of Identity Cholesky decomposition (RICD) approximation.[26] For the single-ion properties of the Ln^{III} ion in complex **4**, and **5**, the other paramagnetic ion in the respective complexes was replaced with the diamagnetic La^{III} analogue. The Dy^{III} ion has a $4f^9$ configuration and possesses a $^6H_{15/2}$ ground state, while Tb^{III} ion has $4f^8$ configuration with $^7F_6$ ground state. We have computated 21 spin-free sextet states for complexes **1**, and **4** using an active space of CAS (9,7). In the next step we have mixed these CASSCF computed spin-free states via the SO-RASSI module to obtain the spin-orbit states.[27] Similar to this for complex **2**, and **5** we have computed 7 spin free septets, 140 spin free quintets, and 195 spin free triplets for Tb^{III} ions. But, here we have mixed only 7 septets, 78 quartets, 27 triplets states in RASSI module to obtain the spin-orbit states. In the last step, the SINGLE ANISO module was used to extract the g-values, crystal field parameters, transition magnetic moments, magnetic susceptibility, and magnetization of individual Ln^{III} ions in both complexes from these calculated spin orbit states.[28] Finally, the magnetic exchange

interaction (dipolar + exchange contribution) between the Ln^{III} centers in complexes **4**, and **5** was calculated using the POLY ANISO module.[29] Additionally, the good match between our calculated molar magnetic susceptibility and molar magnetization and experimental findings gives the computed values more assurance. The more details of calculated relative energies of spin-free states, spin-orbit states, and g-values are provided in the Supporting Information section.

The magnetic exchange interaction in complex **6** was computed using SR-DFT (scalar relativistic density functional theory) computational technique at the B3LYP[30] level of theory on ORCA/5.0.3 The Douglas-Kroll-Hess (DKH) approximation was used to address scalar relativistic effects.[31] In this case, we used an all-electron scalar relativistic (SARC) basis set for Gd^{III} together with DKH reconstructed versions of def2-type basis sets, and DKH-def2-SVP for the rest of the atoms as implemented in ORCA code. Dispersion corrections were incorporated by Grimme's dispersion and Becke-Johnson damping (D3BJ).[32] To speed up the calculations, resolution-of-identity-chain-of-sphere (RIJCOSX) formalism was employed.[33] The broken-symmetry DFT calculations were performed by flipping the spin on one Gd^{III} center using the spin-flip approach as implemented in ORCA. The broken-symmetry calculations were verified by analyzing the spin-desity on individual Gd^{III} atoms. The exchange coupling was computed with the formula – $\boldsymbol{J} = -\frac{E_{HS} - E_{BS}}{2S1\,S2 + S2}$

Table S11. BS-DFT computed energies of high-spin and broken-symmetry solution, spin densities, and *J* values complex **6**.

Solutions	**Energy (Hartree)**	ρ^{Gd}	ρ^{Gd}	$\langle S^2 \rangle$	***J*** **(cm^{-1})**	**J for Dy^{III} (= J*25/49)**	***J forTb^{III} (= J*36/49)***
HS	-31296.557390685437	7.025	7.024	56.0120	-0.019	-0.009	-0.014
BS	-31296.55739160294	-7.017	7.016	7.0120			

J values are estimated using the following equation,

$$J = -\frac{E_{HS} - E_{BS}}{2S1S2+S2}$$

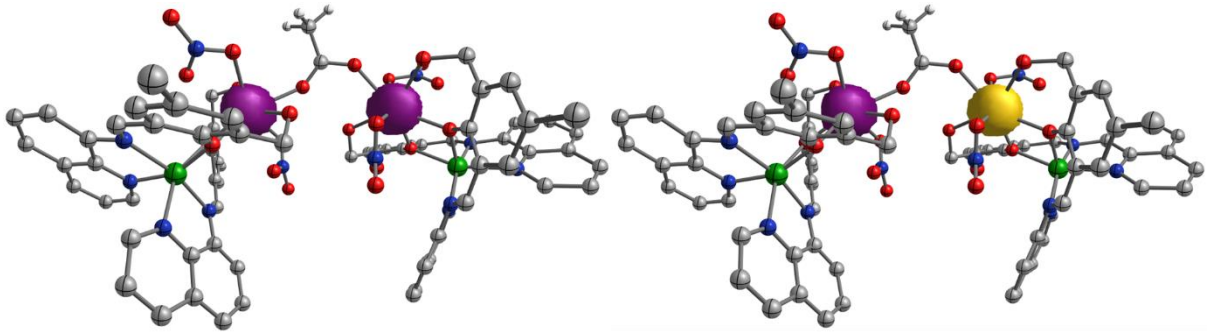

Figure S30: DFT computed spin-density plot of; (a) High Spin (S = 7); (b) Broken Symmetry (S = 0) of complex **6**. The purple and yellow Color represent the positive and negative spin density respectively, with an isosurface value of 0.01 e^-/bohr^3. (Color code: Gd -olive; Zn -Green; O -red; N-blue; C-grey; H-white).

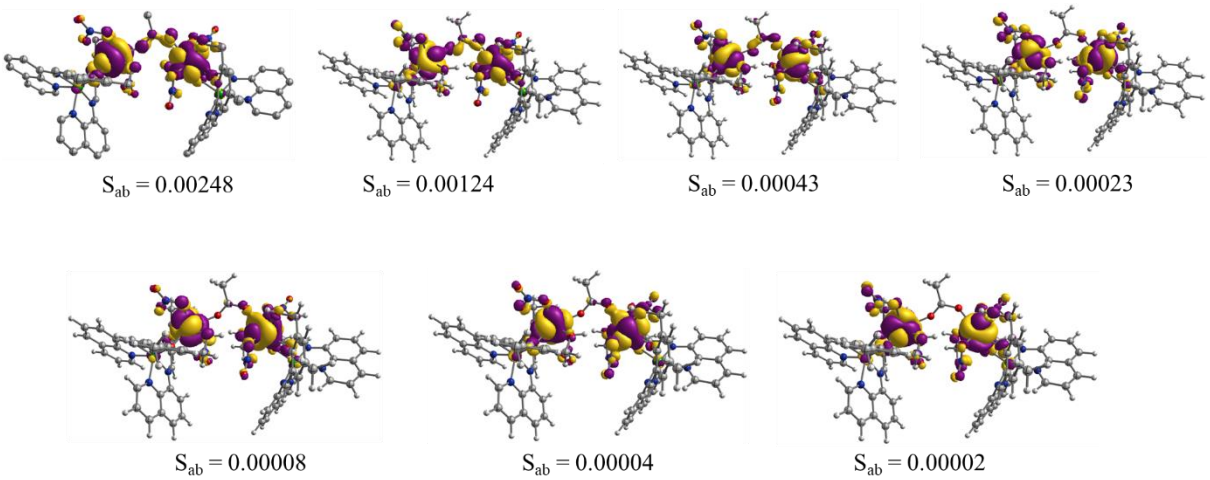

Figure S31. DFT computed corresponding orbitals for which the overlap integral values were calculated complex **6** at contour value = 0.01 e-/bohr^3. (Color code: Gd -olive; Zn -Green; O -red; N-blue; C-grey; H-white).

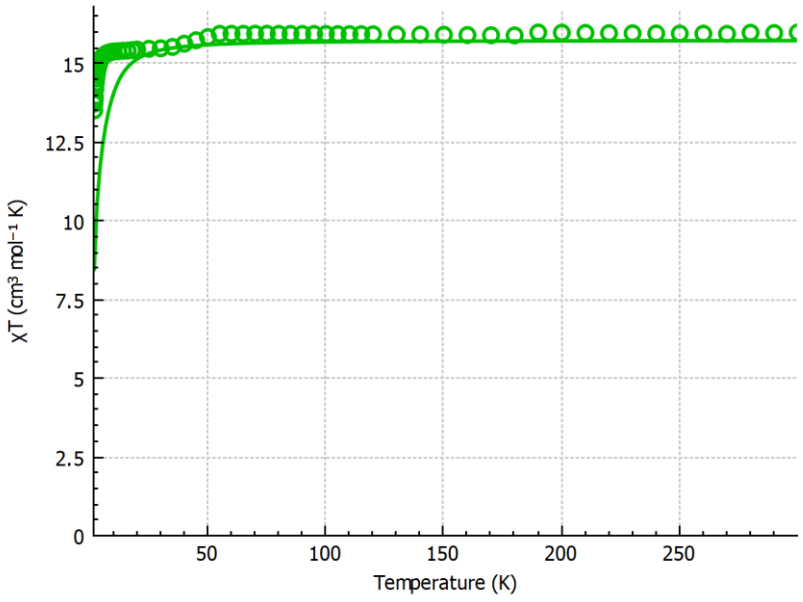

Figure S32. Temperature dependence of χT products for complex **6** under a dc field of 1000 Oe. The green solid lines are simulated simultaneously by using PHI software.

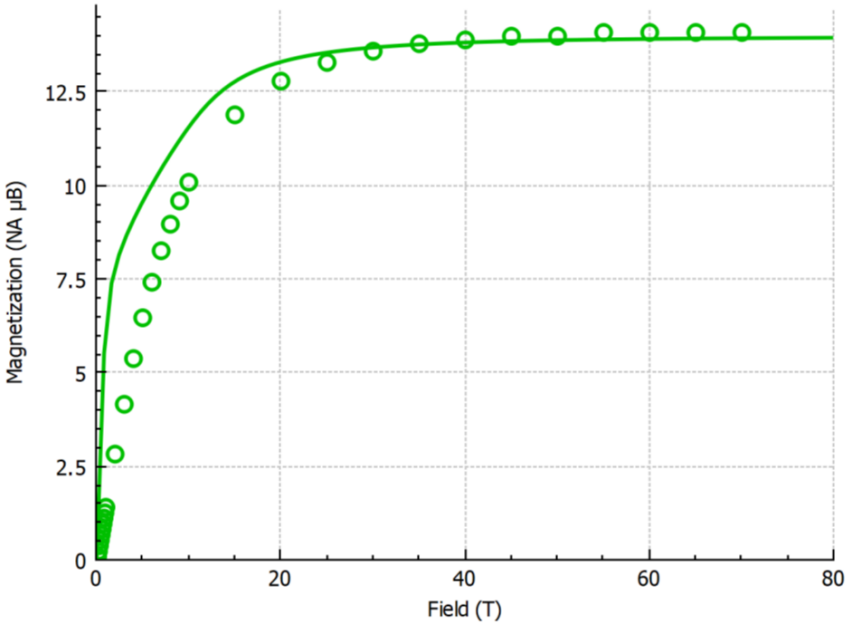

Figure S33. Field dependence of the magnetization data at 2K for complex **6**. The green solid lines are simulated simultaneously by using PHI software.

Table S12. SINGLE_ANISO computed g-tensors, the angle of deviation from ground state g_{zz} orientation, and relative energies of eight low lying Kramers' doublets for Dy center in trimer complex **1**.

KDs	Energy (cm^{-1})	g_{xx}	g_{yy}	g_{zz}	θ
1	0.0	0.0020	0.0030	19.9322	
2	127.1	0.0188	0.0231	17.1657	5.4
3	236.9	0.2907	0.4016	14.0287	8.2
4	286.0	0.1009	0.5559	17.8642	72.5
5	309.9	4.6691	5.8436	8.9062	33.0
6	356.4	2.8158	3.9664	13.8858	86.7
7	404.5	0.4929	0.8254	18.9721	89.9
8	620.4	0.0067	0.0121	19.7944	63.2

Table S13. SINGLE_ANISO computed g-tensors, the angle of deviation from ground state g_{zz} orientation, and relative energies of low lying SOC states for Tb center in trimer complex **2**.

KDs	Energy (cm^{-1})	g_{xx}	g_{yy}	g_{zz}	θ
1	0.0	0.0000	0.0000	17.7162	
	0.5				
2	156.1	0.0000	0.0000	14.0441	5.4
	163.6				
3	272.6	0.0000	0.0000	10.2207	7.8
	307.3				
4	353.7	0.0000	0.0000	6.6713	30.3
	397.2				
5	405.3				
6	463.7	0.0000	0.0000	14.1891	97.6
	468.0				
7	568.6	0.0000	0.0000	16.3429	103.5
	569.1				

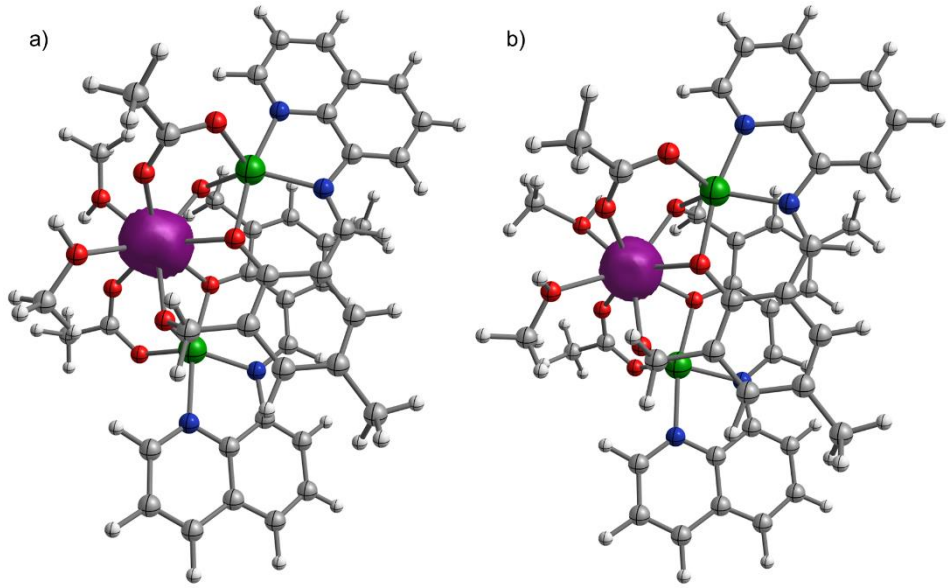

Figure S34. SINGLE_ANISO computed β - spin density for trimer a) complex **1** and b) complex **2** at contour value = 0.003 e-/$bohr^3$. (Color code: Dy -Magenta; Tb -Teal; Zn -Green; O -red; N-blue; C-grey; H-white)

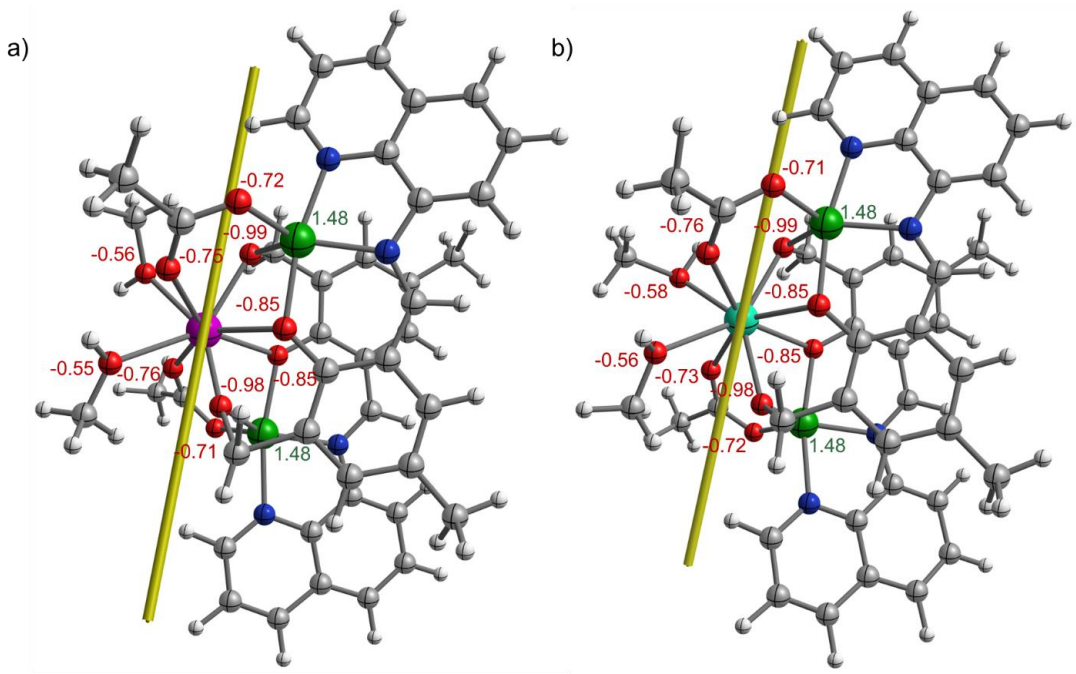

Figure S35. CASSCF computed LoProp charges on the first coordinating atoms of Dy center in trimeric (a) complex **1**; Tb center in (b) complex **2** respectively. (Color code: Dy -Magenta; Tb -Teal; Zn -Green; O -red; N-blue; C-grey; H-white).

Table S14. SINGLE_ANISO computed g-tensors, the angle of deviation from ground state g_{zz} orientation, and relative energies of eight low lying Kramers' doublets for Dy@1 and Dy@2 centers in tetramer complex **4**.

Dy@1					**Dy@2**				
Energy (cm^{-1})	g_{xx}	g_{yy}	g_{zz}	**θ**	**Energy (cm^{-1})**	g_{xx}	g_{yy}	g_{zz}	**θ**
0.0	0.0485	0.0855	19.7674		0.0	0.0489	0.0916	19.7362	
106.6	0.7007	1.3639	16.1131	6.4	116.6	0.6683	1.1128	16.2383	6.3
169.1	2.3399	3.4843	11.3745	11.0	203.4	2.2186	3.3760	11.7014	17.9
229.8	3.2380	5.7900	9.2231	91.7	257.4	2.9692	5.0811	12.8213	93.8
305.4	1.5628	2.1953	11.4225	84.8	325.5	1.3390	2.0744	11.8399	89.0
444.9	0.0820	0.1201	14.9364	80.0	487.3	0.0155	0.0337	14.7801	92.3
513.5	0.0241	0.0330	19.2017	88.1	578.4	0.0051	0.0089	19.6589	92.1
681.2	0.0035	0.0060	19.6386	90.6	637.1	0.0020	0.0182	18.0748	93.6

Table S15. SINGLE_ANISO computed g-tensors, the angle of deviation from ground state g_{zz} orientation, and relative energies of eight low lying Kramers' doublets for Tb@1 and Tb@2 centers in tetramer complex **5**.

		Tb@1				**Tb@2**			
Energy (cm-1)	g_{xx}	g_{yy}	g_{zz}	**θ**	**Energy (cm-1)**	g_{xx}	g_{yy}	g_{zz}	**θ**
0.0	0.0000	0.0000	17.7608		0.0	0.0000	0.0000	17.8081	
0.4					0.3				
127.5	0.0000	0.0000	14.3093	2.1	160.7	0.0000	0.0000	14.3628	0.9
131.2					164.4				
225.6	0.0000	0.0000	10.6293	7.6	282.9	0.0000	0.0000	10.4699	6.0
229.9					292.8				
287.8					352.4				
327.0	0.0000	0.0000	10.3038	91.5	411.3	0.0000	0.0000	10.5496	88.0
346.5					424.6				
428.8	0.0000	0.0000	14.4320	90.2	529.6	0.0000	0.0000	14.5994	89.8
431.8					531.5				
719.1	0.0000	0.0000	17.8238	89.0	850.2	0.0000	0.0000	17.8291	94.5
719.2					850.3				

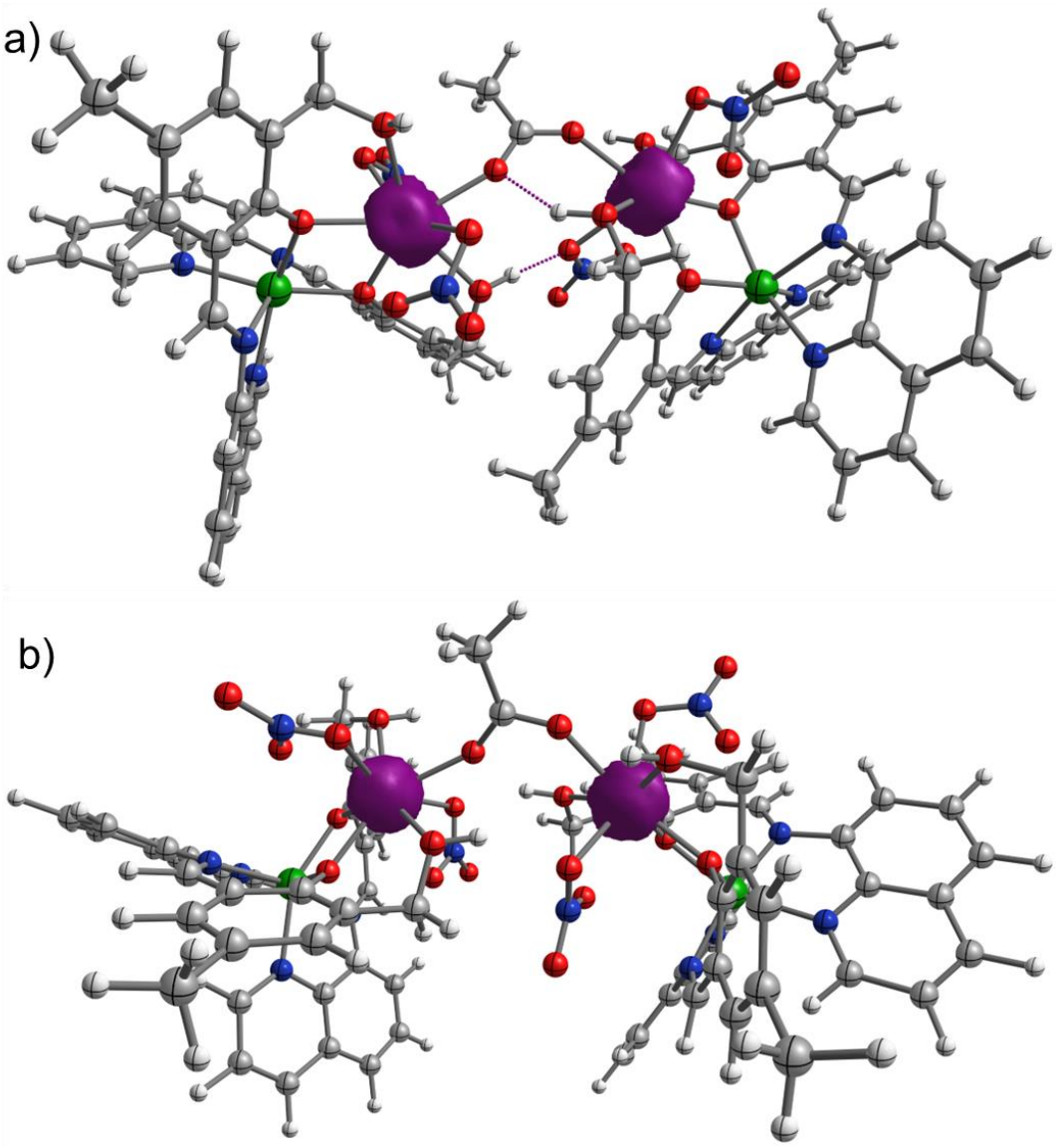

Figure S36. SINGLE_ANISO computed β - spin density a) complex **4** and b) complex **5** at contour value = 0.01 e-/bohr^3 (Color code: Dy -Magenta; Tb -Teal; Zn -Green; O -red; N-blue; C-grey; H-white).

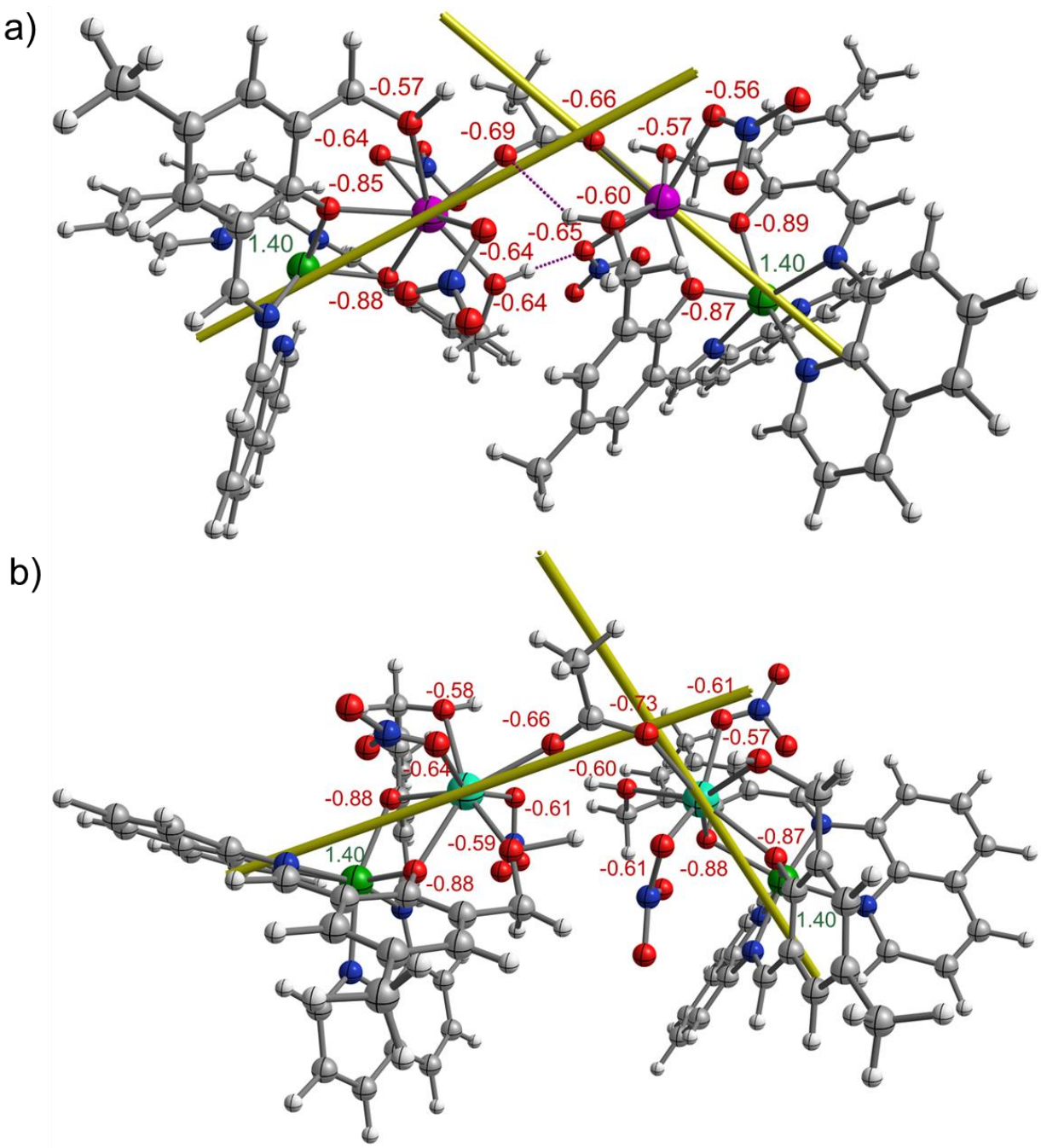

Figure S37. CASSCF computed LoProp charges on the first coordinating atoms of Dy centers in complex **4** b) Tb centers in complex **5** (Color code: Dy -Magenta; Tb -Teal; Zn -Green; O -red; N-blue; C-grey; H-white).

Table S16. Exchange and dipolar interaction were obtained from the POLY_ANISO simulation from the best fit using the Lines model for **4**.

J_{tot}	J_{ex}	J_{dipo}	z_J
-0.80	-0.801	0.001	-0.002

Table S17. Energies of the low-lying non-Kramers' exchange doublets along with gzz and tunneling gap obtained from POLY_ANISO simulation for **4**.

Exchange doublet	**E (cm^{-1})**	**g_{zz}**	**Δ_{tunnel}**
1	0.0	21.8677	5.1E-04
2	3.0	32.6200	2.9E-04
3	106.8	19.4383	7.8E-03
4	109.5	30.0406	4.8E-03
5	116.5	18.5788	5.2E-03
6	119.7	30.9126	3.1E-03
7	223.3	15.8667	8.3E-02
8	226.1	28.0433	4.6E-02

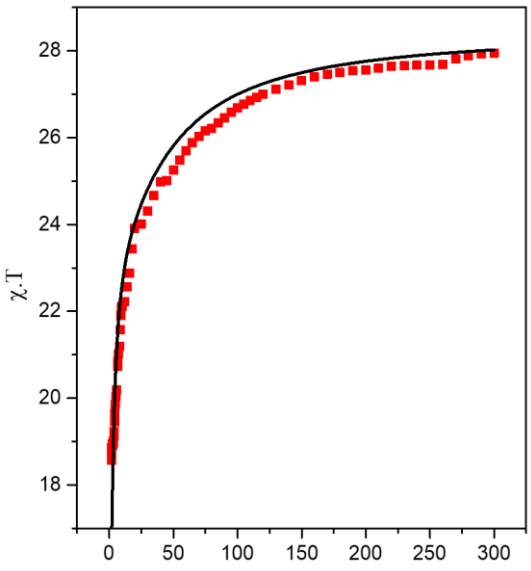

Figure S38. Thermal dependence of the molecular magnetic susceptibility for **1**. The res boxes are the experimental values, while the black line represent the POLY_ANISO simulated data.

Table S18. Exchange and dipolar interaction were obtained from the POLY_ANISO simulation from the best fit using the Lines model for **5**.

J_{tot}	J_{ex}	J_{dipo}	z_J
-0.001	-0.0011	0.0001	-0.002

Table S19. Energies of the low-lying non-Kramers' exchange doublets along with gzz and tunneling gap obtained from POLY_ANISO simulation for **5**.

Exchange doublet	**E (cm^{-1})**	**g_{zz}**	**Δ_{tunnel}**
1	0.1	24.5577	1.5E-01
2	0.7	20.5904	1.5E-01
3	127.8	18.1848	2.9E-01
4	131.5	17.5691	2.9E-01
5	160.9	18.1000	3.5E-01
6	164.7	17.5538	3.5E-01
7	290.1	15.9763	3.5
8	294.0	13.1921	3.5

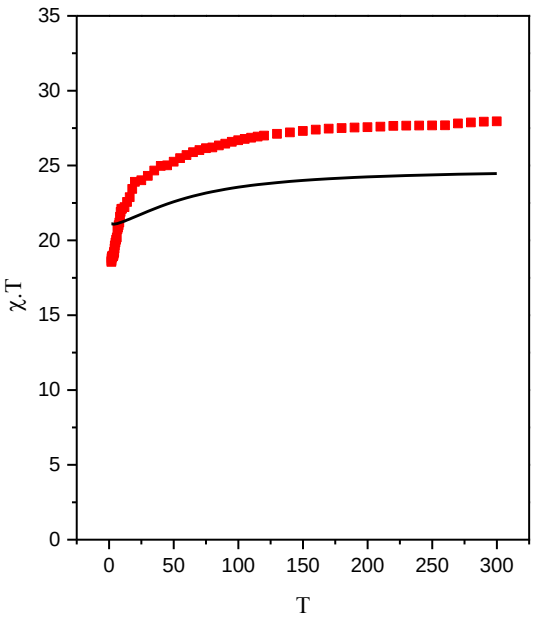

Figure S39. Thermal dependence of the molecular magnetic susceptibility for **1**. The res boxes are the experimental values, while the black line represent the POLY_ANISO simulated data.

Reference

[1] Y. Cui, F. Zheng, Y. Qian, J. Huang, *Inorg. Chim. Acta.* **2001**, *315*, 220-228.

[2] S. Das, K. S. Bejoymohandas, A. Dey, S. Biswas, M. L. P. Reddy, R. Morales, E. Ruiz, S. T.-Padilla, E. Colacio, V. Chandrasekhar, *Chem. Eur. J.*, **2015**, 21, 6449-6464.

[3] P. Shukla, K. U. Ansari, C. Gao, S. Vaidya, S. Tripathi, P. Kumar, R. J. Butcher, J. Overgaard, M. Shanmugam, *Dalton Trans.*, **2020**, 49, 10580-10593.

[4] M. Fondo, J. Corredoira-Vázquez, A. M. García-Deibe, J. Sanmartín-Matalobos, J. M. Herrera, E. Colacio, *Inorg. Chem.* **2017**, 56, 10, 5646–5656.

[5] M. Fondo, J. Corredoira-Vázquez, A. Herrera-Lanzós, A. M. García-Deibe, J. Sanmartín-Matalobos, J. M. Herrera, E. Colacio, C. Nuñez, *Dalton Trans.* **2017**, *46*, 17000-17009.

[6] J. P. Costes, S. Titos-Padilla, I. Oyarzabal, T. Gupta, C. Duhayon, G. Rajaraman, E. Colacio, *Chem. Eur. J.* **2015**, *21*, 15785-15796.

[7] S. Das, K. S. Bejoymohandas, A. Dey, S. Biswas, M. L. P. Reddy, R. Morales, E. Ruiz, S. Titos-Padilla, E. Colacio, V. Chandrasekhar, *Chem. Eur. J.* **2015**, *21*, 6449-6464.

[8] P. Shukla, K. U. Ansari, C. Gao, S. Vaidya, S. Tripathi, P. Kumar, R. J. Butcher, J. Overgaard, M. Shanmugam, *Dalton Trans.* **2020**, *49*, 10580-10593.

[9] E. Echenique-Errandonea, A. Zabala-Lekuona, J. Cepeda, A. Rodríguez-Diéguez, J. M. Seco, I. Oyarzabal, E. Colacio, *Dalton Trans.* **2019**, *48*, 190-201.

[10] S. Titos-Padilla, J. Ruiz, J. M. Herrera, E. K. Brechin, W. Wersndorfer, F. Lloret, E. Colacio, *Inorg. Chem.* **2013**, 52, 9620–9626.

[11] S. Ghosh, N. Hari, D. Pinkowicz, M. Fitta, S. Mohanta, *New J. Chem.* **2018**, *42*, 15917-15929.

[12] H. Yan, C.-M. Wang, P. Chen, Y.-Q. Zhang, W.-B. Sun, *Dalton Trans.* **2022**, *51*, 6918-6926.

[13] *SMART & SAINT Software Reference manuals, Bruker Analytical X-ray Systems, Inc., Madison*, **2003**.

[14] G. M. Sheldrick, *Bruker AXS Inc., Madison, WI SAINT (Version 6.02), SADABS (Version 2.03)*, **2002**.

[15] *SHELXTL, Reference Manual, Ver. 6.1, Bruker Analytical X-ray Systems, Inc., Madison, WI*, **2000**.

[16] K. Bradenburg, *Diamond, Ver. 3.1eM, Crystal Impact GbR, Bonn, Germany* **2005**.

[17] O. V. Dolomanov, L. J. Bourhis, R. J. Gildea, J. A. K. Howard, H. Puschmann, *J. Appl. Crystallogr.* **2009**, *42*, 339-341.

[18] P. van der Sluis, A. L. Spek, *Acta Crystallogr. Sect. A: Found. Crystallogr.* **1990**, *46*, 194201.

[19] A. Spek, *Acta Crystallogr. Sect. A: Found. Crystallogr.* **1990**, *46*, c3.

[20] F. Neese, *Wiley Interdiscip. Rev. Comput. Mol.*, **2022**, *12*, e1606.

[21] a) J. P. Perdew *Phys. Rev. B: Condens. Matter Mater. Phys.*,**1986**, *33*, 8822-8824 b) A. D. Becke *Phys. Rev. A*, **1988**, *38*, 3098.

[22] G. L. Manni, I. F. Galván, A. Alavi, F. Aleotti, F. Aquilante, J. Autschbach, D. Avagliano, A. Baiardi, J. J. Bao, S. Battaglia, L. Birnoschi, A. Blanco-González, S. I. Bokarev, R. Broer, R. Cacciari, P. B. Calio, R. K. Carlson, R. C. Couto, L. Cerdán, L. F. Chibotaru, N. F. Chilton, J. R. Church, I. Conti, S. Coriani, J. Cuéllar-Zuquin, R. E. Daoud, N. Dattani, P. Decleva, C. de Graaf, M. G. Delcey, L. De Vico, W. Dobrautz, S. J. S. Dong, R. L. Feng, N. Ferré, M. Filatov, L. Gagliardi, M. Garavelli, L. González, Y. F. Guan, M. Y.

Guo, M. R. Hennefarth, M. R. Hermes, C. E. Hoyer, M. Huix-Rotllant, V. K. Jaiswal, A. Kaiser, D. S. Kaliakin, M. Khamesian, D. S. King, V. Kochetov, M. Krosnicki, A. A. Kumaar, E. D. Larsson, S. Lehtola, M. B. Lepetit, H. Lischka, P. L. Ríos, M. Lundberg, D. X. Ma, S. Mai, P. Marquetand, I. C. D. Merritt, F. Montorsi, M. Mörchen, A. Nenov, V. H. A. Nguyen, Y. Nishimoto, M. S. Oakley, M. Olivucci, M. Oppel, D. Padula, R. Pandharkar, Q. M. Phung, F. Plasser, G. Raggi, E. Rebolini, M. Reiher, I. Rivalta, D. Roca-Sanjuán, T. Romig, A. A. Safari, A. Sánchez-Mansilla, A. M. Sand, I. Schapiro, T. R. Scott, J. Segarra-Martí, F. Segatta, D. C. Sergentu, P. Sharma, R. Shepard, Y. N. Shu, J. K. Staab, T. P. Straatsma, L. K. Sorensen, B. N. C. Tenorio, D. G. Truhlar, L. Ungur, M. Vacher, V. Veryazov, T. A. Voss, O. Weser, D. H. Wu, X. C. Yang, D. Yarkony, C. Zhou, J. P. Zobel, R. Lindh, *J. Chem. Theory Comput.*, **2023**, *19*, 6933-6991.

[23] B. O. Roos, P. R. Taylor, P. E. M. Sigbahn, *Chem. Phys.*, **1980**, *48*, 157-173.

[24] B. O. Roos, V. Veryazov, P.-O. Widmark, *Theor. Chem. Acc.*, **2004**, *111*, 345-351.

[25] B. O. Roos, R. Lindh, P.-Å. Malmqvist, V. Veryazov, P.-O. Widmark, A. C. Borin, *J. Phys. Chem. A*, **2008**, *112*, 11431-11435.

[26] F. Aquilante, R. Lindh, T. Bondo Pedersen, *J. Chem. Phys.*, **2007**, *127***,** 114107.

[27] P. Å. Malmqvist, B. O. Roos, B. Schimmelpfennig, *Chem. Phys. Lett.*, **2002**, *357*, 230-240.

[28] L. F. Chibotaru and L. Ungur, *J. Chem. Phys.*, **2012**, *137*, 064112.

[29] a) L. F. Chibotaru, L. Ungur, C. Aronica, H. Elmoll, G. Pilet, D. Luneau, *J. Am. Chem. Soc.*, **2008**, *130*, 12445-12455. b) L. F. Chibotaru, L. Ungur, A. Soncini, *Angew. Chem., Int. Ed.*, **2008**, *47*, 4126-4129. c) L. Ungur, W. Van den Heuvel, L. F. Chibotaru, *New J. Chem.*, **2009**, *33*, 1224-1230.

[30] A. D. Becke, *J. Chem. Phys.*, **1993**, *98*, 5648-5652.

[31] B. A. Hess, *Phys. Rev. A*, **1986**, *33*, 3742-3748.

[32] a) S. Grimme, J. Antony, S. Ehrlich, H. Krieg, *J. Chem. Phys.*, **2010**, *132*, 154104. b) S. Grimme, S. Ehrlich, L. Goerigk, *J. Comput. Chem.*, **2011**, *32*, 1456-1465.

[33] J. M. Guevara-Vela, T. Rocha-Rinza, Á. M. Pendás, *Theor. Chem. Acc.*, **2017**, *136*, 57.